PhotoMOB: Automated GIS method for estimation of fractional grain dynamics in gravel bed rivers.

Part 2: Bed stability and fractional mobility

A Preprint

October 26, 2023

Fanny Ville [1] ,**Colin. D. Rennie** [2], **Ramon. J. Batalla** [1,3], **Damià Vericat** [1,4]

[1]Fluvial Dynamics Research Group (RIUS), University of Lleida, Lleida, Spain

[2]Department of Civil Engineering, University of Ottawa, Ottawa, Ontario, Canada

[3]Hydrological Processes Area, Catalan Institute for Water Research, Girona, Spain

[4]Forest Sciences and Technology Centre of Catalonia, Solsona, Spain

Contact details of the corresponding author:

Fanny Ville, University of Lleida, Alcalde Rovira Roure, 191, E-25198 Lleida, Catalunya, Spain

Email: fanny.ville@udl.cat

Abstract

Bed mobility and stability are spatially and temporally variable, making it a complex phenomenon to study. This paper is the second of a pair, in which we present an automated image processing procedure for monitoring the mobility/stability of gravel river beds. The method is based on local comparison of the shape of the grains identified at the same coordinates between successive photos to identify coincident and new grains. From this categorisation in a given study area, several variables can be extracted, such as: the general proportion of *mobile* or *immobile* grains (number or area), the maximum *mobile* or *immobile* diameters, the proportion per grain fraction of grains that remained *immobile* (stable) and grains newly identified. Additionally, percentiles of the surface Grain Size Distribution (GSD) before and after a target hydrological event, as well as the *immobile* and *mobilized* GSD (which could be used as a proxy for bedload GSD) can be computed. In this part 2 paper, we present the entire GIS-based procedure for identifying the shape of each grain in digital images of bed patches to then classify their dynamic status (*mobile*/*immobile*), and derive a reliable result compatible with different forms of sampling (Area-by-number, Abn, and Grid-by-number, Gbn) and types of measurements (continuous and discrete square holes grain size reading). The performance of the GIS procedure is evaluated for the mentioned above variables over a control set composed of ten 1×1m paired before/after image samples representing different field conditions. The automatic classification applied on a perfect (*manual*) grain delineation yields Mean Absolute Errors (MAE) lower than 3% in both Abn and Gbn, while the automatic classification applied on an *automated* delineation with 10 min of manual boundary *revision* shows MAE around 8% and presents a larger MAE of 29% for only the estimation of the *mobile* percentile.

Keywords: Particle dynamics, Bed stability, Fractional mobility, GIS, Fluvial monitoring, River habitat

1 Introduction

Riverbed stability and mobility, referring to the bed surface that remains stable or not (MacKenzie et al., 2018), varies over time and space. The understanding, characterization, and prediction of bed surface dynamics related to sediment transport is important for geomorphologists (e.g., estimation of transported or deposited volume) and ecologists (e.g., the timing and intensity of bed instability determines the disturbance of aquatic substrate habitats and thus controls the presence and resilience of aquatic organisms (e.g., Cobb et al., 1992; Matthaei and Townsend, 2000; Gibbins et al., 2005, 2007).

A first approach to evaluate the mobility (or the loss of stability) of grains is based on the competence of the flow (Gilbert and Murphy, 1914) by estimating the force of the water required to set into motion grains present on the bed (e.g., Miller et al., 1977; Komar, 1987; Ashworth et al., 1992; Parker, 2008; Dey and Ali, 2019). For a given force exerted on the bed, (i) the mobility can be defined as equal when all the grain fractions are movable independently of their size (ii) while it is selective when only certain grain fractions enter into motion. The mobilization is generally positively dependent on the grain size (an increase in force will progressively mobilize coarser grains). This approach is commonly based on the observation and measurement of the coarsest clasts mobilised for different competent hydrological events (Andrews and Parker, 1987). Although this method is sometimes also used by ecologists (e.g., Downes et al., 1997; Duncan and Suren, 1999; Lorang and Hauer, 2003), it has a disadvantage as a *mobile* grain of a given size does not necessarily mean that all grains of that size are mobilised.

Another approach to characterizing substrate mobility, based on the proportion of surface and bedload grain fractions, has been introduced by Wilcock and McArdell (1993) and further used by, for instance, Wathen et al. (1995), Wilcock (1997), Mao and Lenzi (2007). When the proportion of a grain fraction of diameter *i* present in the bedload is the same to that of the bed surface, then the term full mobility can be used. When the proportion of a given size fraction present in the bedload is less that of the bed the surface, then the mobility can be termed partial.

To feed these two cited example approaches, one inexpensive method, with respect to both instrument cost and fieldwork effort, is the use of tracers such a painted bed area (see summary in Hassan and Roy (2016)). A representative area of the bed is painted and photographed. After a hydrological event, a repeated photograph of the initial patch can be taken and the entrained painted grains can be eventually located downstream and transport distances measured, as well as their size (e.g., Church and Hassan, 2002; Hassan and Ergenzinger, 2003; Vericat et al., 2008; Mao et al., 2017 ; Brenna et al., 2019; Vázquez-Tarrío et al., 2019; Vericat et al., 2020). This method avoids altering natural grain imbrication and packing without limitation of tracer size.

However, mobilised painted grains can be transported over varying distances and may settle on the paint side down and/or be subsequently buried, resulting in a low recovery rate. For example, in the context of a hydropeaked river generating limited mobility (i.e., intensity and size range) especially emphasizing the finest fractions López et al. (2023), the mobility of the latter, difficult to visually detect downstream, may be consequently be poorly characterized (size and distance). Furthermore, the number of grains found in relation to the number of grains initially painted is not known. Most measurements focus on the downstream particles, while a large amount of information from the original spot location is usually not exploited, such as the proportion of the bed surface that is stable (*immobile*) or not (*mobile*) for each grain size fraction. This information is present on the photographs; hence, an analysis based on all the grains present in the photos (before and after), not just on the few grains found downstream, would greatly increase the number of particles studied and potentially improve the accuracy of deduced trends of dynamics.

To our knowledge, this information has not been systematically extracted. There is thus the need for an automated systematic photographic measurement method that is reproducible and easily implemented to quantify fractional stability and mobility (e.g., Peckarsky et al., 2014; Gibbins, 2015; Quinlan et al., 2015). Photographs collected from many different areas of the bed (bar head, low and high bar, secondary channels) would then enable examination of the spatial and temporal variability of bed grain stability or entrainment and transport by fraction. In addition, new particles deposited on the study surface may be included in the analysis of the next hydrological event without having made any additional effort in the field other than the acquisition of a new photo. In order to draw on the data set provided by repeated photographic acquisition (Cerney, 2010) of patches, we developed a GIS-based method that allow a spatial grain-by-grain inter-analysis of the particles present in the two sets of photographs.

This paper is the second of a pair of papers in which we describe and evaluate this methodological procedure. The first paper dealt with the workflow under GIS environment to perform identification and characterisation of grains in digital images of gravel river beds, to derive reliable surface Grain Size Distributions (GSD). In this second paper, we first describe the workflow to categorize the dynamics of each grain, then we present a performance evaluation with a non-optimal photo set corresponding to various complex field conditions (limited time available, imperfect photo shooting, partially wet surface due to flooding or hydropeak, etc.). Finally, we discuss the application of the method, as well as limitations and recommendations to extract the most accurate results. In the course of this article, all the references to "Text **S**", "Table **S**", and "Figure **S**" followed by a number indicate the location of the element in question in the supplementary material section.

2 The complete PhotoMOB workflow

The objective of the PhotoMOB procedure is to compare two photos, of the exact same river bed area, acquired before and after a hydrological event (or a succession of events when it is impossible to access the area – Figure 1 A. The process consists of two parts: i) the first, the grain detection; only a brief description of the identification procedure is given below (for a detailed explanation, the reader is referred to companion paper Part 1); ii) the second step, the categorization, allows the classification of each particle as *mobile* or *immobile* by a spatial grain-by-grain comparison (Figure 1 D).

2.1 Grains' detection

The photos are (i) first filtered with the successive use of a high pass filter and two noise reduction filters using GIMP (Team, 2019), an image manipulation program, to improve edges contrast and smooth the intra-grain noise. This first step improves the detection of the particles. (ii) Then, the initial filtered photo (pre-event) is loaded into ArcGIS© to be manually scaled using the distance between the four internal corners of the frame as reference points. A projective transformation is applied. The second photo (post-event) is then georeferenced to the first. This alignment is done manually by identifying identical points between the two photos. This step should be done as accurately as possible. Again, a projective transformation is applied. It is mandatory that the images are well aligned with each other, as a slight misalignment may not allow a correct superposition of the grains, which may result in a *mobile* grain classification even in the case of the same grain in the identical position. (iii) The two photos are then automatically processed with the *PhotoMOB toolbox part 1* to extract the contour of each grain as a polygon shapefile (see companion paper, Part 1). (iv) At this stage, if the photos present some complexity (e.g., variation of sunlight, partially wet, heterogeneous lithology, partially painted, presence of vegetation), it is advisable to check the result of the grain delimitation and edit them manually, if necessary, as errors of delimitation are likely to occur. From this image processing it is then possible, at each time step, to know the surface GSD of the *a* and *b* particle axes as *continuous* data and not by class, the orientation with respect to the north of the photo, as well as the proportion of fine material (fine limit defined by the operator).

2.2 Characterization of grain dynamics

The second part of the method classifies each detected particle as (i) *mobile* or (ii) *immobile* by comparing the superposed pre (T0) and post-event (T1) photos on a grain-by-grain basis (Figure 1 D and Figure **S**1 C). This is carried out in two steps: (i) calculation of a geometric shape descriptor at pre- and post-event times, and (ii) classification of the mobility status.

2.2.1 Hypothesis and rationale

Categorization is based on the following hypothesis: if two particles, sharing approximately the same xy coordinate on the two pre- and post- event images, are identical, then they are considered to be the same *immobile* particle i.e., not having been mobilized during the hydrological event. On the other hand, if their shapes are relatively different (according to a certain threshold) then they are not the same, which may indicate particle *mobilization* during the hydrological event.

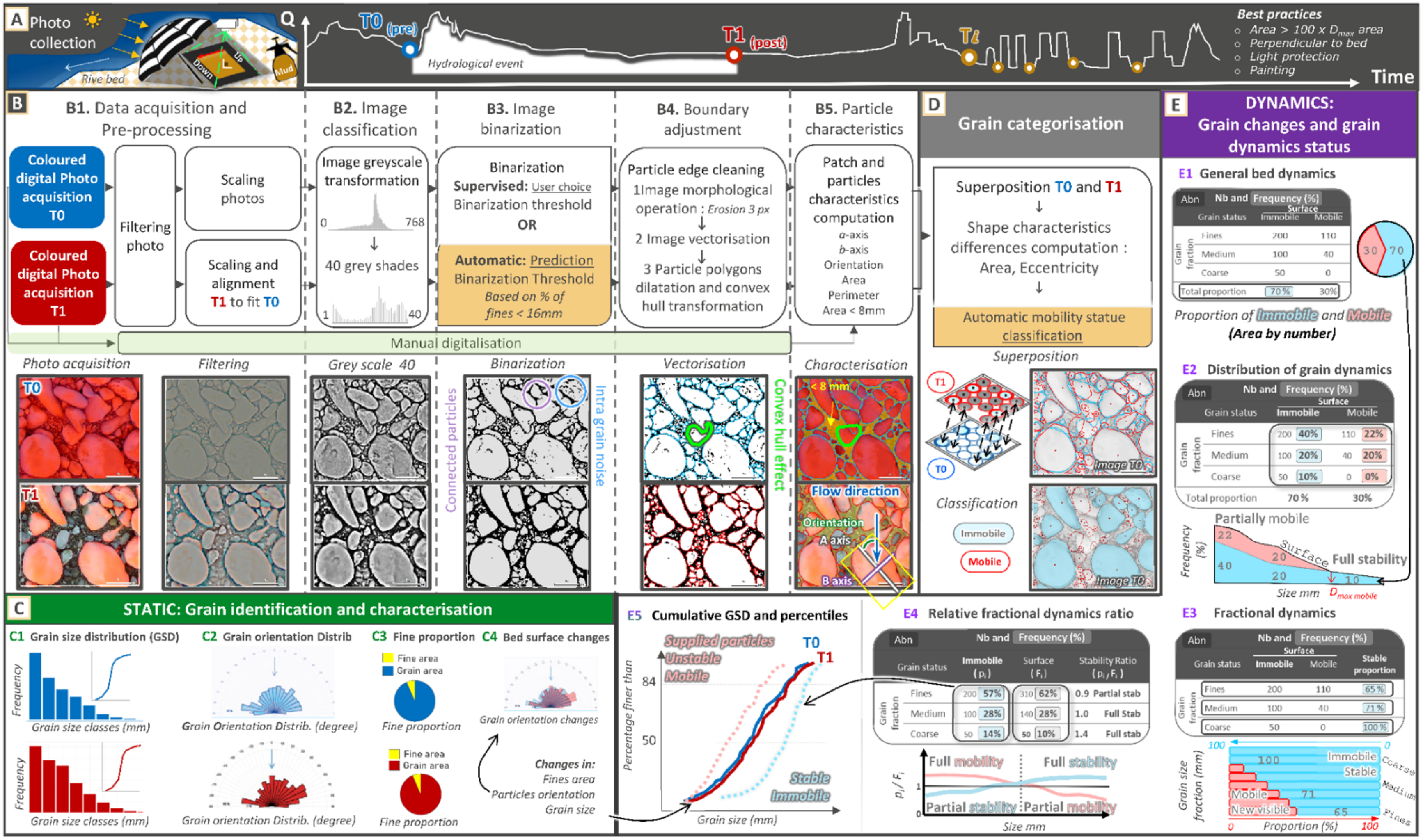

Figure 1: Illustration of the entire workflow required to characterize bed surface (see companion paper, Part 1) and sediment dynamics (developed in this paper). (A) Photo acquisition. (B) Detection of grain and patch characteristics. (C) Possible output after patch surface characterisation. (D) Characterisation of dynamics and (E) conceptual example of possible output from dynamics characterisation. The rounded black-edged rectangles in the tables represent the whole on which the proportions are calculated. For example, the 200 fine *immobile* particles represent 40% of all visible surface particles (E2), 65% of all fine fraction surface particles (E3), and 57% of all *immobile* particles (E4). The yellow boxes represent the developed models (i) of dark threshold prediction (companion paper) and (ii) of particle classification (see in text).

With the classification, from the pre-event time (T0) photo, *stable immobile* particles can be identified that are still in place (still visible), as well as the *unstable* area formed by the particles that are no longer visible on the surface and which correspond either to particles mobilized (eroded) during the event or covered by new ones. Similarly, from the post-event photo (T1), *stable immobile* grains during the event (i.e., identical particle between both images) can be identified, and new particles that are now visible on the surface either because they were mobilized and deposited in the study area or because they were uncovered due to localized erosion of the surface. As such, if the particle is not the same between the pre-event (T0) and post-event (T1) photos, then either or both of the particles visible in images T0 and T1 were mobilized during the event.

Of course, the categorization has limitations that the user should keep in mind, concerning our basic hypothesis and the classification terminology used (*immobile*/*mobile*), which may be wrong in some cases. The concept of stability/instability can by more attributed to the description of the sampled surface, while the concepts of immobility/mobility to the grain. By clarifying the notion of stability/instability, immobility/mobility,Section 5.2 will show that this criticism can be in some way minimised.

2.2.2 Workflow

A unique ID is assigned to each grain in the two layers. Then, each pair of superposed particles is selected Figure 1 D. For this purpose, the centre of the polygon particle at T1 is marked with a point, still containing T1 shape information. Then, to this point layer, is coupled by spatial join, the information of the T0 particle polygon layer of which this point is located above. If a T1 particle is not coupled to any T0 particle, then it is considered to be *mobile* (*newly arrived*). At this stage, the analysis consists of a layer of points with the attributes of both pre- and post- particles present at the same location. The particles are classified according to their relative degree of likeness. The classification of the dynamics status of each particle as *mobile* or *immobile* is done automatically from a classification model developed over ten pairs of 40 x 40 cm photos where 1704 grain pairs were identified, classified, and used to train the model (details in Text S.2.2 and Figure **S**1). The classification tree of dynamics is shown in Figure 2. If two paired particles have a difference in area greater than 38%, then they are considered to be different (*mobile*). If not, if the difference in eccentricity is greater than 31%, then they are considered to be mobile, otherwise they are identical (*immobile*).

From the point layer containing the classification, the dynamics status is returned to both polygon layers via an attribute-based join based on the grain identifiers. If no match is found for a particle at T0 then it is considered *mobile*.

Once the particles have been classified, it is possible to derive different types of information. These data can be expressed as the number of grains in the sampled area, i.e., Area-by-number (Abn), or in terms of grain area in the sampled area. The latter is equivalent to the Grid-by-number (Gbn) data form commonly obtained by the pebble-count method (Wolman, 1954). The reader is invited to refer to Figure 1 E and Text S.2.2 for a conceptual example of the data that can be obtained from the photo pair analysis.

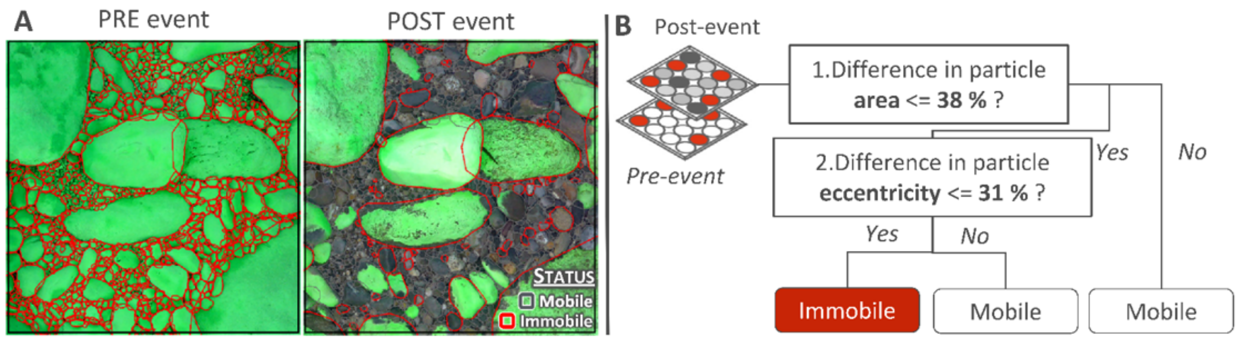

Figure 2: Classification tree of dynamics, developed on 1704 visual grain comparison. (A) Example of one of the sample patch used to build (B) the decision tree. The two photos were digitised manually and a visual mobility classification was then carried out on the second photo.

3 Performance assessment

The goodness of the dynamics characterization is highly dependent on (i) the classification model we have developed and (ii) the correct grain boundary delimitation. The objective is to obtain an automated classification of all particles as *immobile* or *mobile* as it could be done by the eyes of a human operator, but much faster. In this section we will present a control data set and quantify the errors on the E1 to E5 outputs shown in Figure 1.

In addition, we also wish to quantify how much of the error is due to the classification model and how much is due to boundary errors detection.

3.1 Control dataset

The control data-set was obtained from two gravel-bed rivers of the South Central Pyrenees (Cinca and Ésera). The sedimentary characteristics of these rivers are detailed in the companion paper (Part 1). Pre- and post- image pairs for hydrological events of various magnitudes (natural floods, hydropeaks), and different from the training set of the classification model, were selected in order to introduce variability in particle lithology, shape, interlocking and mobility degree. All of the control data images were collected at similar elevation and with direct sunlight protection. Figure 3 A shows the set of 10 pairs of photos taken with direct sunlight protection but with a mixture of photo conditions (painted and unpainted, partially wet, partially painted). The pairs of photos T0 and T1 never correspond to the same condition and sometimes the paint on the painted patch photos got relatively dissolved which allows the asperities of the particles to show through (S4 or S6). It should be noted that these photos are from previous field campaigns and were not acquired specifically for developing *PhotoMOB*.

For each pair of photo samples (a small view shown in Figure 3 A), an area of interest of 1 m² was defined. As shown in the classification model, all particles present within these zones were delimited by hand. This represents a total of 15080 particles. Partially buried particles were included where it was possible to identify them with certainty between the two photos. The overlapping particles at T1 and T0 were listed in a point shapefile. Finally, a single operator visually assigned the status (*immobile* or *mobile*) to each listed T1 particle. Approximately 7480 visual pairwise comparisons were conducted. If the centroid of a particle at T1 was located above more than one T0 polygon, which could occur because a convex hull was applied to smooth the contours of the particles, then the T1 particle was deemed to be *mobile* only if it differed from all associated particles in T0.

The control data set was therefore acquired with a *manual* delineation followed by a visual classification. The characteristics of the sampled area of the post-surface truncated at 8 mm are presented in Table 1 while the cumulative GSDs of the pre-surface, post-surface, *mobile* and *immobile* are presented in Figure 3 B and the frequency distribution per grain fraction in Figure 3 C.

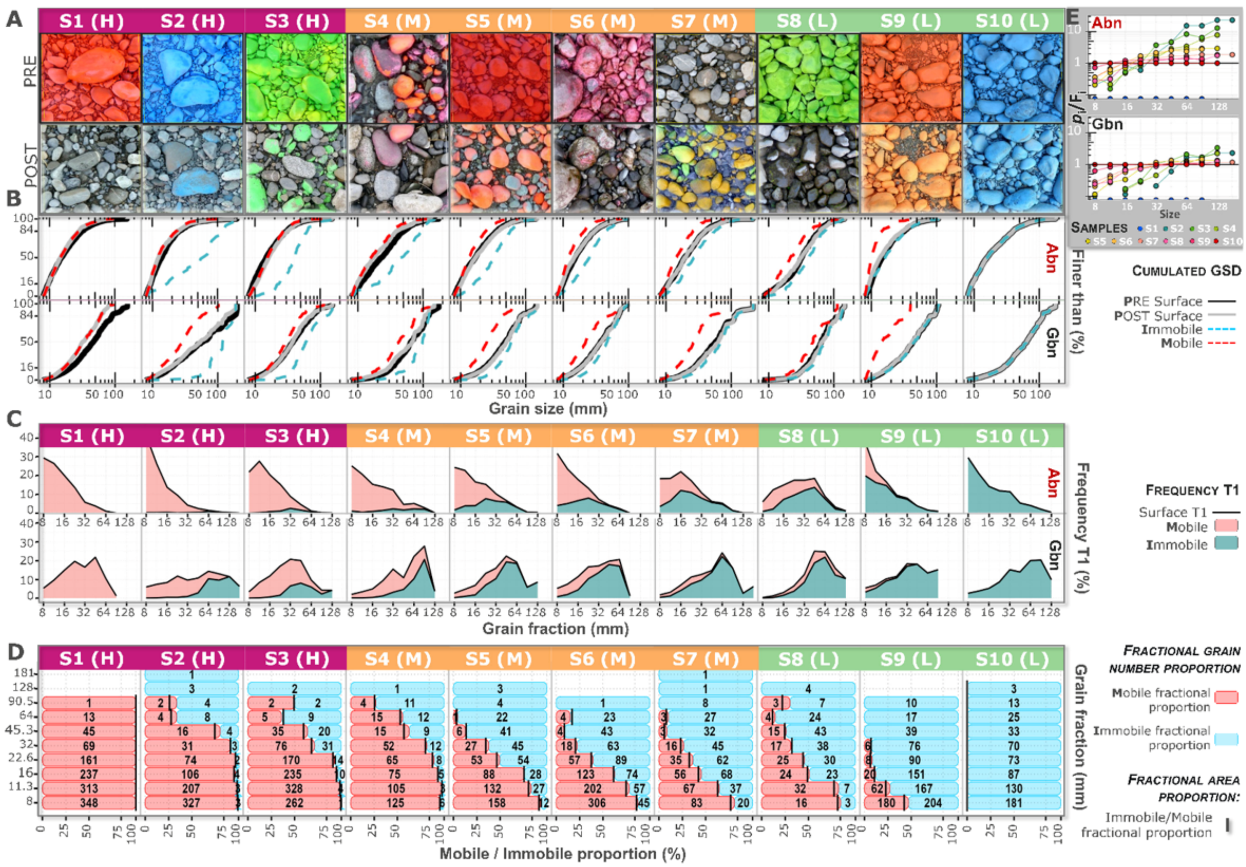

Figure 3: Control dataset used to test the particle dynamics image-processing procedure, obtained by *manual* delimitation and visual classification of each grain. (A) Zoom on a portion of $1m^2$ squares of T0 (pre-event) and T1 (post-event) of the ten samples. (B) Cumulative grain size distribution of each sample in Area-by-number (Abn, first row) and Grid-by-number (Gbn, second row) truncated at 8 mm. The solid black and grey curves indicate the GSD at T0 and T1 respectively. The dashed red and blue curves indicate the *mobile* and *immobile* GSD respectively. (C) Stacked distribution frequency of *mobile* (red area) and *immobile* (blue area) grains in each grain fraction of size 0.5ψ, based on the classification obtained with the T1 layer; the black line at the top thus represents the distribution frequency of all surface grains visible at T1. The first row corresponds to the data in Abn form and the second in Gbn. (D) Fractional dynamics. Percentage of *mobile* (red) and *immobile* (blue) particles number found on the post-event surface for each grain fraction. The numbers in bold correspond to the number of grains of each status in each fraction. The black vertical marks indicate the *mobile* and *immobile* proportion area for each fraction. Relative fractional stability in Abn (top) and Gbn (bottom). Stability ratio $p_{i\ immobile}$ $/F_i$ as a function of grain fraction. Where p_i is the proportion of each size fraction *i* present in the whole *immobile* grain category and F*i* is the proportion of each size fraction *i* in the whole surface bed sediment.

Table 1: Characteristics of the control samples

Sample	River	Photo condition Pre[a]	Photo condition Post[a]	$D_{84\,immo}/D_{84\,surf}$	D_{max} (mm)	Stability % Grain	Stability % Area	Mobility Status[c]	Nb total	8–11.3	11.3–16	16–22.6	22.6–32	32–45.3	45.3–64	64–90.5	90.5–128	128–181	181<	D5 Abn	D5 Gbn	D16 Abn	D16 Gbn	D50 Abn	D50 Gbn	D84 Abn	D84 Gbn	D95 Abn	D95 Gbn
S1 (H)	Cinca	C1	C2	Inf	93	0	0	$Surface_{T1}$	1187	348	313	237	161	69	45	13	1	0	0	9	11	10	16	15	32	28	60	45	77
								Immobile	0	0	0	0	0	0	0	0	0	0	0	-	-	-	-	-	-	-	-	-	-
								Mobile	1187	348	313	237	161	69	45	13	1	0	0	9	11	10	16	15	32	28	60	45	77
S2 (H)	Cinca	C0	Mix C1C1	4.6	190	4	43	$Surface_{T1}$	802	330	210	110	76	34	20	12	6	3	1	8	11	9	18	12	54	25	132	46	190
								Immobile	35	3	3	4	2	3	4	8	4	3	1	9	52	17	75	59	119	118	187	166	190
								Mobile	767	327	207	106	74	31	16	4	2	0	0	8	10	9	13	12	28	23	57	36	96
S3 (H)	Ésera	C0	Mix C1C1	2.1	152	8	29	$Surface_{T1}$	1206	263	332	245	184	107	55	14	4	2	0	9	12	10	18	16	38	31	73	48	113
								Immobile	93	1	4	10	14	31	20	9	2	2	0	16	31	23	39	41	60	64	120	88	152
								Mobile	1113	262	328	235	170	76	35	5	2	0	0	9	11	10	16	15	30	27	51	40	80
S4 (M)	Ésera	Mix C1C2 WET	Mix C1C2	1.9	149	13	44	$Surface_{T1}$	523	131	108	80	73	64	24	27	15	1	0	9	16	10	29	18	68	39	106	74	133
								Immobile	67	6	3	5	8	12	9	12	11	1	0	9	33	20	59	45	98	98	123	120	149
								Mobile	456	125	105	75	65	52	15	15	4	0	0	9	13	10	22	16	43	34	78	56	114
S5 (M)	Cinca	C0	Mix C1C1	1.6	150	34	73	$Surface_{T1}$	701	170	159	116	107	72	47	23	4	3	0	9	14	10	24	17	51	38	84	61	146
								Immobile	236	12	27	28	54	45	41	22	4	3	0	11	24	16	35	32	60	59	111	80	150
								Mobile	465	158	132	88	53	27	6	1	0	0	0	8	10	10	14	14	25	24	44	36	62
S6 (M)	Ésera	C1	Mix C1C1	1.5	98	36	68	$Surface_{T1}$	1109	351	259	197	146	81	47	27	1	0	0	9	11	10	18	15	39	30	70	51	82
								Immobile	395	45	57	74	89	63	43	23	1	0	0	10	18	12	26	25	47	46	73	67	87
								Mobile	714	306	202	123	57	18	4	4	0	0	0	8	9	9	12	12	22	21	49	31	71
S7 (M)	Ésera	Mix C1C2	Mix C1C2 WET	1.4	217	53	84	$Surface_{T1}$	564	103	104	124	97	61	35	30	8	1	1	9	16	11	27	19	64	41	113	72	217
								Immobile	301	20	37	68	62	45	32	27	8	1	1	11	20	15	32	27	69	56	121	82	217
								Mobile	263	83	67	56	35	16	3	3	0	0	0	9	10	10	14	14	26	26	48	38	76
S8 (L)	Ésera	C1	C2 WET	1.2	146	57	78	$Surface_{T1}$	315	19	39	47	55	55	58	28	10	4	0	11	25	15	37	31	66	62	125	86	141
								Immobile	179	3	7	23	30	38	43	24	7	4	0	16	28	22	44	41	74	72	128	106	146
								Mobile	136	16	32	24	25	17	15	4	3	0	0	10	16	12	28	21	48	46	93	65	113
S9 (L)	Cinca	C0	Mix C1C1	1.1	107	73	93	$Surface_{T1}$	1030	384	229	171	98	82	39	17	10	0	0	8	11	9	19	14	43	30	81	52	103
								Immobile	754	204	167	151	90	76	39	17	10	0	0	9	13	10	21	16	46	35	93	57	103
								Mobile	276	180	62	20	8	6	0	0	0	0	0	8	9	9	10	10	14	14	34	23	40
S10 (L)	Cinca	C1	C1	1	177	100	100	$Surface_{T1}$	615	181	130	87	73	70	33	25	13	3	0	8	14	9	28	16	64	39	114	70	166
								Immobile	615	181	130	87	73	70	33	25	13	3	0	8	14	9	28	16	64	39	114	70	166
								Mobile	0	0	0	0	0	0	0	0	0	0	0	-	-	-	-	-	-	-	-	-	-

[a] Photographic condition, *C1*: protected from the sun and fully painted, *C2*: Protected from the sun and not painted, *WET*: area partially wet, *Mix C1C2*: protected from the sun and partially painted. [b] ratio of the D84 for the *immobile* grain and the bed surface at T1 in Abn. [c] presentation of all grains composing the surface in T1, those identified as *immobile* and those *mobile*. [d] percentiles in Area-by-number and Grid-by-number. Grid-by-number extraction from the identified grains follows the method described in Graham et al. (2005b) and in the companion paper

The 10 samples were classified into 3 groups according to their degree of bed disturbance (see (see Table 1). Samples 1 to 3 were classified as having high mobility intensity with a ratio $D_{84\,Immobile}/D_{84\,Surface} > 2$. There were no or very few particles that remain *immobile*, with mostly large particles making up the *immobile* group. Samples 4 to 7 were classified as having a medium mobility intensity with a ratio of $1.2 < D_{84\,Immobile}/D_{84\,Surface} < 2$. Finally, samples 8 to 10 were classified as having low mobility, as few or no *mobile* particles were identified. The ratio $D_{84\,Immobile}/D_{84\,Surface} < 1.2$ indicates a surface almost identical to the *immobile* grains. The samples are presented from highest to lowest degree of mobility.

Figure 3 B shows that some samples, such as S5, S6, S7 and S8, do not have significantly different pre and post GSDs (black and grey solid curve Figure 3 B) (p-value of K-S test > 0.05) although surface changes have occurred. The distributions are presented as both Abn and Gbn to demonstrate the importance of the choice of distribution form. Furthermore, for a given sample, the calculated stable bed proportion (blue area in Figure 3 C) is not the same whether one uses the number of *immobile* grains (Abn) or the area covered by *immobile* grains (Gbn). For example, sample S4 contains 13% of *immobile* grains whereas in terms of surface area covered by *immobile* grains, the stability is 44% (see Table 1).

The fractional dynamics of each sample is shown in Figure 3 D. The red horizontal columns represent the proportion of the number of *mobile* grains for each fraction. The *immobile* proportion is represented by the blue columns. The boundary between these two columns thus indicates the distribution of grains as *mobile* or *immobile* within each fraction. Regardless of the sample and the corresponding intensity, the few grains above 128 mm are fully *immobile*. The vertical black bars indicate the proportion of *mobile* and *immobile* grains in terms of surface area. These black bars are located at very near the red and blue column boundaries (on average 2% difference), because Abn and Gbn distributions are essentially the same for fractional mobility since all particles within a narrow grain size class are of the same size.

Finally, an overview of the relative fractional stability is presented in Figure 3 E. In Abn, this figure shows that for high intensity events (S1 to S4) the grains larger than 32 mm are very over-represented in the *immobile* group. The ratio is between 5 and 25. In comparison, grains smaller than 16 mm are very under-represented or even absent, indicating they were very *mobile*. In Gbn, the four high intensity samples show grains over-represented only for fractions > 64 mm, with ratios between 1 and 3. This figure shows that in Gbn only large fractions can be classified as relatively fully stable, whereas in Abn, intermediate size fractions are also considered as relatively fully stable with larger ratios than in Gbn. In contrast to fractional stability, relative fractional stability is dependent on the form of the chosen distribution (Abn or Gbn).

3.2 Performance assessment approaches

To evaluate the performance of *PhotoMOB*, we applied our classification model to three particle delimitation procedures.

(1) The classification model was applied to our *manually* delineated control data set. The control particles and the *manual* tested particles are exactly the same. This evaluates only performance of the classification model, on a different data set from the one used to train the classification model.

(2) The automatic classification was applied to *automatically* delineated particles (Part 1 of the toolbox, developed in the companion article). The proportion of images occupied by material smaller than 16 mm, an input required to run the process fully automatically, was derived from the *manual* delineation. The operator is not expected to know the proportion of material smaller than 16 mm, but must make a visual estimate (we were looking for consistency in the delimitation process). Our classification model was then applied to these *automated* delineations. This permits assessing the magnitude of the combined errors of the delimitation and the classification model. It should be noted that with *automated* delineation the control particles and the tested particles are not the same. The number of *automated* detected particles differs from the number of control particles by about 20% as already described in the performance analysis of the companion paper (Part 1).

(3) Finally, in order to understand the positive impact that a fast correction of the *automated* delineations by an operator could have, a correction of the *automated* delineation in a maximum time of ten minutes for each of the 20 images was performed by a single operator. This correction consisted mainly in (i) eliminating the over-segmentation areas by selecting then deleting the incorrect multiple small polygons and then redrawing correctly as single polygons, and (ii) fixing under-segmented areas by quickly segmenting as many polygons representing clusters of grains as possible within the time limit. The classification model was then applied to these *reviewed* delineations.

Figure 4 shows an overview of the *automated* particle delineation results at T0 (before-event) and T1 (after-event) (columns A and B), as well as the result of applying the classification model to the *automated* delineation at T1, with the photo at T0 in the background (column C). This figure shows the challenge of the different image conditions. The slightest error in delineation, if not identical on the two photos T0 and T1, will inevitably cause more particles to be classified as *mobile*. On the S4 sample (first row), both photos show partially removed paint and wet areas. The granitic particle in the upper left is present in both photos, but in T1 it is poorly delineated, over-segmented (O). This lead to the classification of a large number of small *mobile* particles which in reality do not exist (M). Sample 6 (second row), shows in T1 the paint was almost completely removed, leaving the problematic asperity of some particles, as well as partially wet areas (W), respectively creating over- and under-segmentation. Finally, sample S9 (last row) shows better photographic conditions, even if in T1 the photo is only partially painted. Nonetheless, some particles are united (U). This problem of under-segmentation comes from the fact that the contrast of the overlapping particles is not strong enough. During classification, this problem may add a higher proportion of *mobile* particles compared to the control set, mainly in the large fractions. The same figure but with the *reviewed* delimitation is available in Text S.3.2 and Figure **S**2.

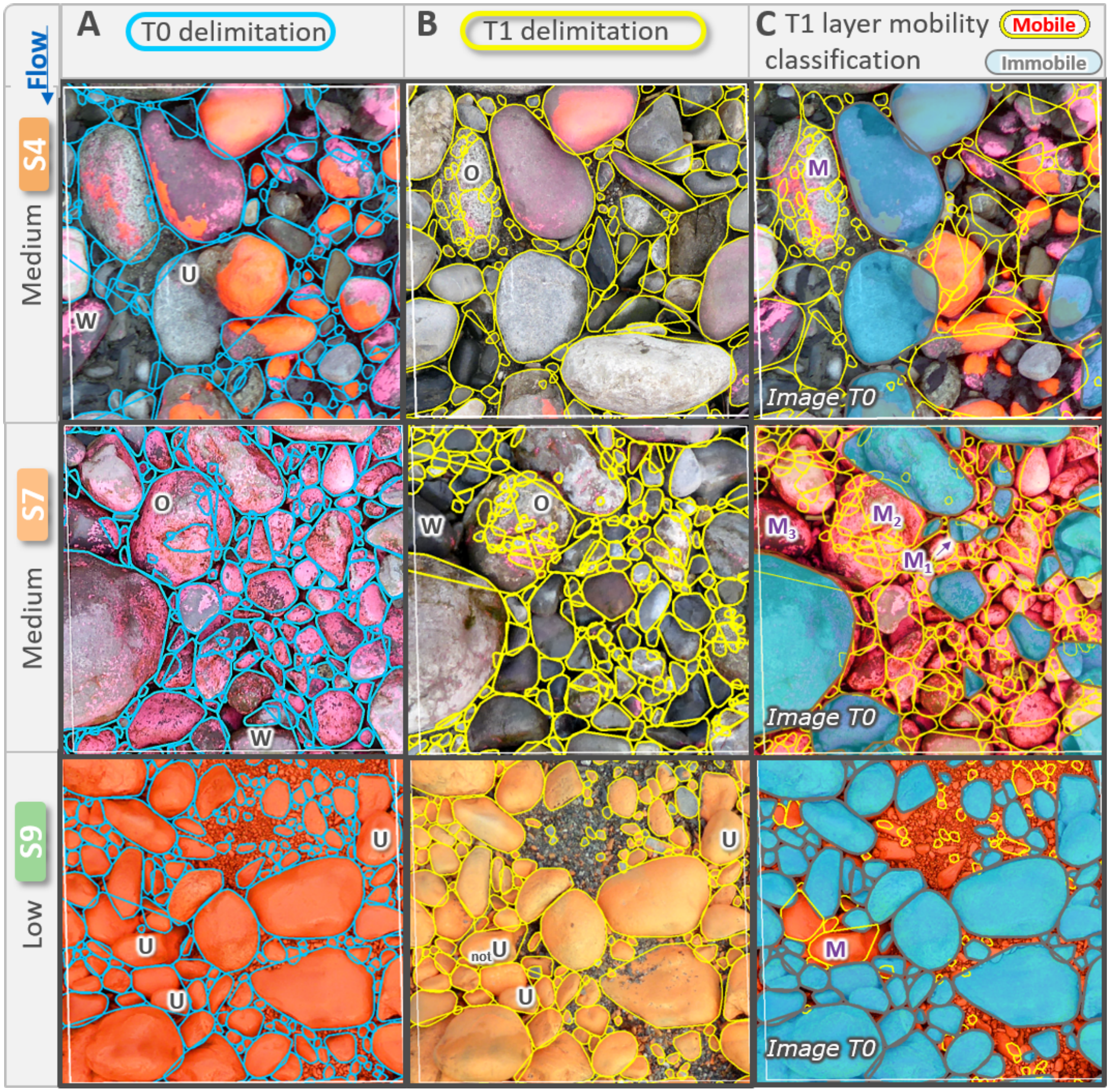

Figure 4: article delineation results at T0 (A) and T1 (B) by automated image-processing procedure. (C) Automated particle classification as *immobile* or *mobile* based on T1 classification. The image patches represent approximatively 0.4×0.4 m and show detected particles >8mm. The `U` labels denote examples of under-segmentation issues, the `O` labels denote examples of over-segmentation issues, the label `w` denotes examples of wet surface generating under-segmentation leading to *non-real* large particle and the label `M` shows misclassification examples. `M1` corresponds to a misclassification as *immobile* due to similar shape; `M2` corresponds to misclassification of many *non-real* small particles as *mobile*; and `M3` corresponds to a larger *non-real* particle misclassified as *mobile*.

For the 10 control post-event (T1) distributions, and for the three tested image processing procedures, we calculated different variables in Abn and Gbn form:

(E1) the proportion (%) of bed stability (inversely proportional to bed mobility), , corresponding to output E1 in Figure 1 E.

(E2) the frequency distribution (%) in grain fractions ($F_{8,\ 11.3,\ 16,\ 22.6,\ 32,\ 45.3,\ 64,\ 90.5,\ 128,\ 181}$) per mobility status ($F_{i\ Immobile}$, $F_{i\ Mobile}$), corresponding to output E2 in Figure 1 E and visible in Figure 3 C.

(E3) for each size fraction, the proportion that was classified as *immobile* and *mobile* ($P_{i\ Immobile}$, $P_{i\ Mobile}$), corresponding to output E3 in Figure 1 E and in Figure 3 D.

(E4) the relative stability and mobility ratio for each grain fraction ($R_{i\ Immobile}$, $R_{i\ Mobile}$),corresponding to output E4 in Figure 1 E.

(E5) 15 common percentiles ($D_{5,\ 10,\ 16,\ 20,\ 25,\ 30,\ 40,\ 50,\ 60,\ 70,\ 75,\ 80,\ 84,\ 90,\ 95}$) of the *immobile* and *mobile* grain size distribution have been extracted ($D_{i\ Immobile}$, $D_{i\ Mobile}$), corresponding to output E5 in Figure 1 E. The method of the extraction of percentiles in the form Gbn is developed in the companion paper.

We chose to evaluate the performance using the classification obtained with the post-event layer (T1), but it would also have been possible to perform this analysis based on the classification obtained in pre-event (T0). This aspect is discussed in 5.2 and 5.3.

Residuals between control and tested value

$$Residuals = Var_{i\,predicted} - Var_{i\,control}$$

have been calculated for the approaches E1 to E3, error ratios

$$Error\ Ratio = Var_{i\,predicted}/Var_{i\,control}$$

for the E4 approach, and finally the relative residuals

$$Relative\ Residuals = (Var_{i\,predicted} - Var_{i\,control}) \times 100/Var_{i\,control}$$

regarding percentile estimates (E5).

As in the companion paper using the residuals and relative residuals (E1, E2, E3 and E5), four metrics were applied to quantify the estimation error over the 10 samples: the root mean square error, the irreducible random error, the bias (B), indicating whether the evaluations were on average over- or under-estimated, defined as : $B_{Var\,i} = \frac{1}{n}\sum(Residuals_i)$, where *n* represents the number of patches (10) and the mean absolute error (MAE), corresponding to the reducible error or the error of accuracy, indicating how far from the correct value are the estimates, given as: $MAE_{Var\,i} = \frac{1}{n}\sum(|Residuals_i|)$. For the error ratios concerning the E4 approach, only an average of the error ratios for each of the 10 grain size fractions is calculated. Finally, the error of the procedures for each approach (E1 to E5) was quantified by calculating for each metric its average over all variable elements *Var* i:

$$Procedure\,performance_{metrics} = \frac{1}{n} * \sum(Metrics_{Var_i} + Metrics_{D_{Vari+1}} + ... + Metrics_{D_{Vari+n}}) \tag{1}$$

where *n* represents the number of studied elements (10 for grain fractions and 15 for percentiles).

The procedure performances in Abn and Gbn for each approach are summarized in Figure 5 . For clarity only the average MAE is presented in this paper. The columns (grey, white and black) represent the average MAE. The dots indicate the average MAE for each sample intensity group. This is indicative of the residuals dispersion of results across groups. Average performance procedure metrics (RMSE, e, Bias, MAE) are available Text S.4.

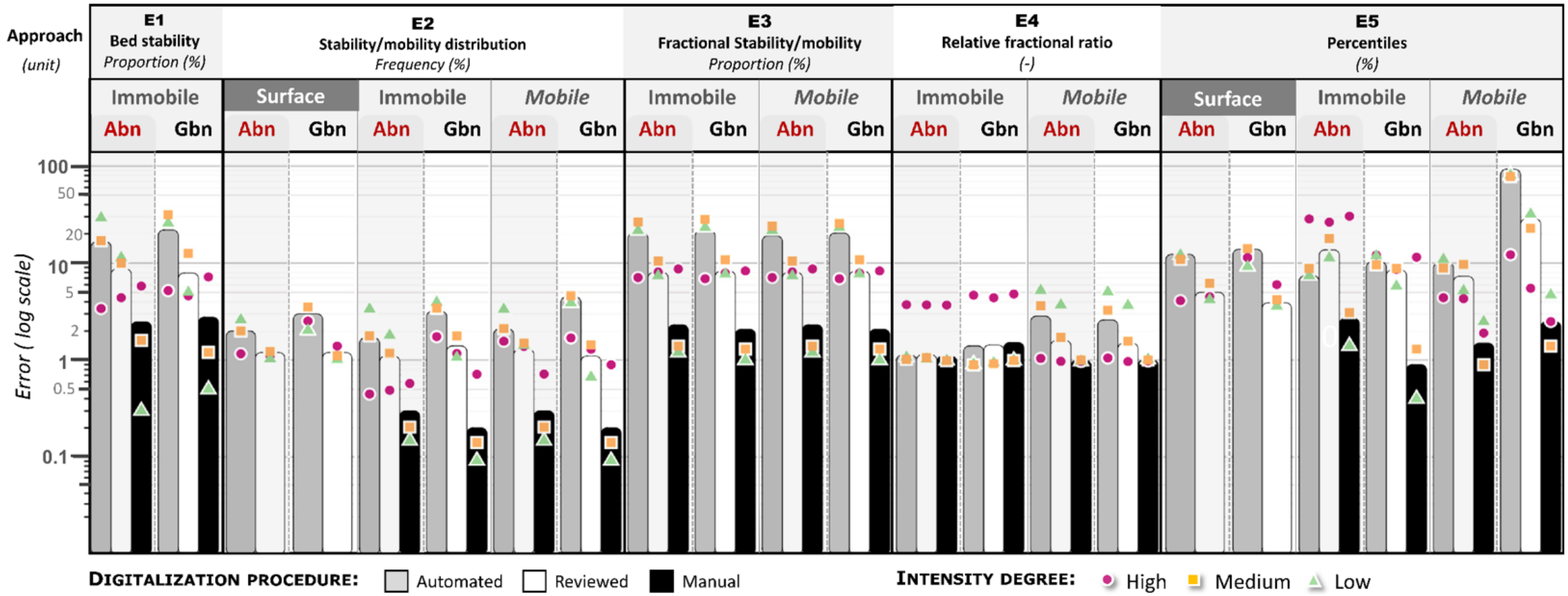

Figure 5: Accuracy and precision performance for the three delineation procedures followed by automatic grain classification for each approach E1 to E5. The performance is presented for each grain category (Surface, *Immobile*, *Mobile*) and in the two forms Abn and Gbn. The colour of the bars corresponds to the delineation procedure (*automated*, *reviewed*, *manual*). The evaluation of the accuracy of the procedures is represented by the average bed stability error between the 10 samples (E1), the average MAE of all grain fractions between the 10 samples (E2) and between the 8 samples S2 to S9 (E3), the average of the mean error ratio of all fractions between the 8 samples S2 to S9 (E4), and finally the average of the relative MAE of all 15 percentiles calculated between the five samples S5 to S9. The assessment of the precision of the procedures is given by the dispersion of the average MAE (E1, E2, E3, E5) or the average error ratio (E4) between the groups of intensity samples. The shape and colour of the dots correspond to the three degrees of mobility (high, medium and low).

When evaluating the average MAE for fractional stability/mobility (E3) and relative fractional stability/mobility (E4) we made the decision to not consider the two extreme samples S1 and S10 presenting respectively *immobile* and *mobile* P_i proportion equal to zero. Moreover, for the percentile estimate average MAE we decided not to consider samples with *immobile* or *mobile* particle size distributions with less than 100 particles (See Table 1). We have thus considered only the 5 samples S5, S6, S7, S8, S9. The reason is that for *immobile* or *mobile* fractions containing little or no grains, inclusion or exclusion of a single particle from a set results in large outlier residuals when compared to the control set, which generates large average percentage errors without reflecting any real trend. However, the behaviour of each procedure on all samples (S1 and S10 included) can be seen in the set of Figure 6 to Figure 8 and dots of average MAE for each sample intensity group take all samples into account in Figure 5.

4 Results of performance assessment

4.1 General bed dynamics

Figure 6 shows the degree of agreement of the bed proportion of the number (Abn) and area (Gbn) of particles classified as *immobile* (or conversely *mobile*) per sample, between the control data (manual delineation + visual classification) and the three delineation procedures (*manual*, *automated*, *reviewed*) followed by the automatic classification. The *manual* delimitation procedure (Figure 6 A shows good agreement for all samples with the control data, for both Abn and Gbn forms. The general MAE taking into account the 3 sample groups is 2.6% (Figure 5 E1 black column). The *automated* procedure presents a less good fit (Figure 6 6B). Bed stability is well estimated for high intensity events. However, there appears to be a larger scatter for samples with lower degrees of mobility. MAEs are more important in Gbn than in Abn, especially for medium intensity events, rising from 17% to 32%. These photos have a high complexity, as for example S4 and S6 in Figure 4, causing coarse *non-real* particles. These *non-real* particles are not present in both paired pictures, so they appear *mobile*. This is more problematic in Gbn because the coarser the particle the more weight it has, whereas in terms of Abn the *immobile*/*mobile* partition is not weighted by the grain surface. Finally, with the *reviewed* delineation, the errors for the medium and low intensity samples are reduced, in both Gbn and Abn, by more than half. The rapid correction of the delineation is obviously localized on the larger polygon's boundaries i.e., coarser *non-real* particles being the most visible.

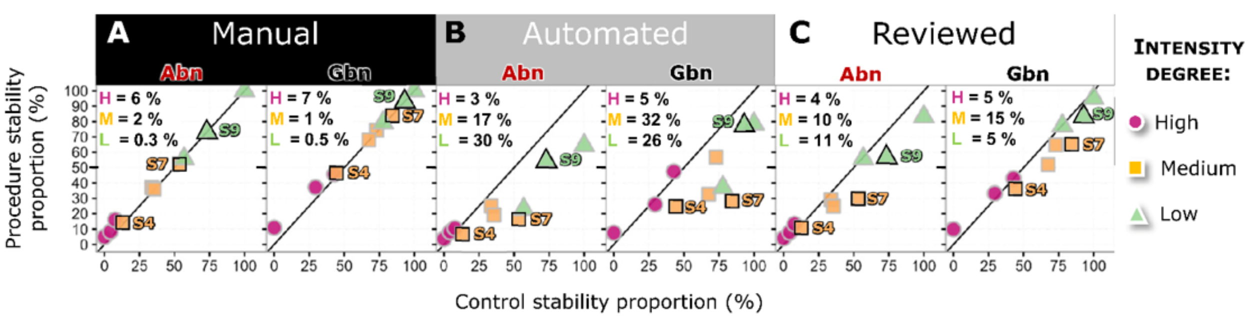

Figure 6: Comparison of the total proportion of grains, in term of number (Abn) and area (Gbn), classified as *immobile* (inversely proportional to *mobile*) for (A) *manual*, (B) *automated* and (C) *reviewed* image-delimitation processing procedure compared to the control. The reference control grain proportion was obtained by a manual digitalisation followed by visual classification. The shape and colour of point correspond to the three mobility degrees (High, Medium Low). Samples taken as examples in @fig-F4 are represented here by black contour. The equality line is shown with a solid bold line. The MAE per sample group is quoted for each procedure.

4.2 Distribution per dynamics status

The frequency distribution prediction errors from the three procedures with the control dataset are presented in Figure 7 , and the percentiles estimates, in both Abn and Gbn form, of the three procedures are shown in Figure 8. Surface percentile estimates for *automated* and *reviewed* procedure at post-event times are shown in Figure 8 A. The *manual* procedure estimate is not presented as the control surface and the manual surface were both obtained manually and thus are composed of the same grains. In part B is presented the *immobile* percentile estimates, and in part C, the *mobile* percentile estimates of the three procedures compared to the control data. The red solid line represents the control data (manual delineation + visual classification), while the black, grey and white points correspond to the predictions obtained via the *manual*, *automated* and *reviewed* delineation procedures respectively followed by automatic dynamics classification.

4.2.1 Identification of surface grains

The errors in the frequency distribution of the grains within each subset ($F_{i\ Immobile}$ and $F_{i\ Mobile}$) are firstly conditioned by a correct delineation of all the surface grains. Figure 7 A shows the post-event surface frequency residuals of each grain fraction for the two forms Abn and Gbn, taking the whole surface sediment as a whole, and Figure 8 A presents percentiles estimation. There appear to be no major differences between the group samples (mobility degrees). The better or worse performance in reproducing the surface distribution is mostly related to the complexity of the photos.

In Abn, the *automated* delineation shows maximum bias of grain frequency of +8% for the particles < 16 mm. Consequently, the particle size distribution of the surface will then tend to be finer than the control due to the presence of small *non-real* particles at the beginning of the distribution, which shifts the distribution towards finer sizes. This phenomenon is illustrated in Figure 8 A. The first row shows the 15 percentile estimates extracted in Abn form for the *automatic* delineation (grey dots) and *reviewed* (white dots) compared to the control set (red solid curve). The grey points tend to lie to the left of the solid curve. The automated procedure average MAE of the percentile estimate is 12.3% (Figure 5 - E5 - Surface -Abn). Eight of the samples have both partially wet and partially painted areas, which creates a large heterogeneity in pixel colour. This average MAE indicates similar performance found in the companion paper for C3 condition (not protected from the sun and not painted), where the average MAE was from 11.2- 14.2%.

In Gbn (Figure 7 A second row Gbn), the *automated* procedure reproduces fairly well frequencies until 64mm, above which there is more scatter and progressively over-estimation by up to 18%. The high surface percentiles will therefore be over-estimated. In Figure 8 A-Gbn (second row), the grey points of the percentiles above D_{75} are often positioned to the right of the red control line. The *automated* procedure average MAE of the surface percentile estimate is 14%. This example shows the importance of the choice of the form to represent the data. The Abn form is likely to have errors in the first fraction while in Gbn the errors seem to be more in the coarse fraction.

The *reviewed* delineation reduces the errors. The *reviewed* procedure average MAE for surface fraction frequency for each sample group in Abn or Gbn is less than 1.4% (see Figure 5 E2 - Surface - white bar), resulting in a *reviewed* procedure average MAE for surface percentile estimate of less than 5%, in both Abn and Gbn (Figure 5 E5 - Surface - white bar). These errors are similar to those found in the companion paper in C1 condition (4.5 to 4.8%).

4.2.2 Stability/Mobility

Figure 7 B and C show the residuals of the grain frequency distribution estimations for each grain fraction per dynamics status, $F_{i\ Immobile}$ and $F_{i\ Mobile}$, concerning the three delineation procedures, while Figure 8 B and D present *immobile* and *mobile* percentiles estimates.

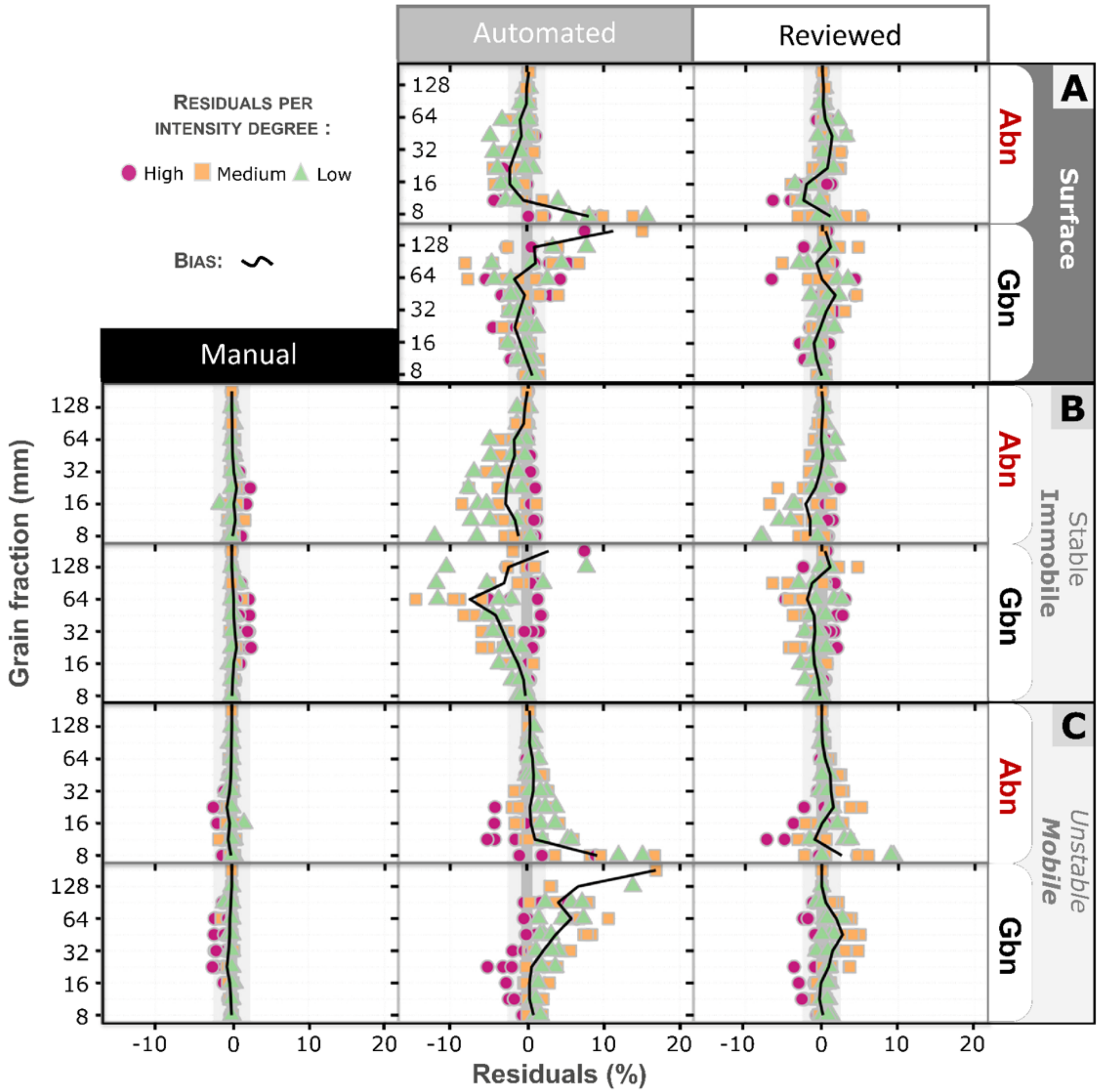

Figure 7: (A) Distribution of the 100 relative post-event surface frequency estimation residuals for the *automated* and *reviewed* delineation procedure (10 samples per 10 grain size fractions). (B) Distribution of the *immobile* and *mobile* (C) Frequency estimation residuals for the *manual*, *automated*, and *reviewed* delineation procedures. The residuals are shown for the forms Abn and Gbn. The shape and colour of point correspond to the three mobility degrees (High, Medium and Low). The bias (mean error across 10 residuals) along grain fraction (%) is shown with the bold black curve.

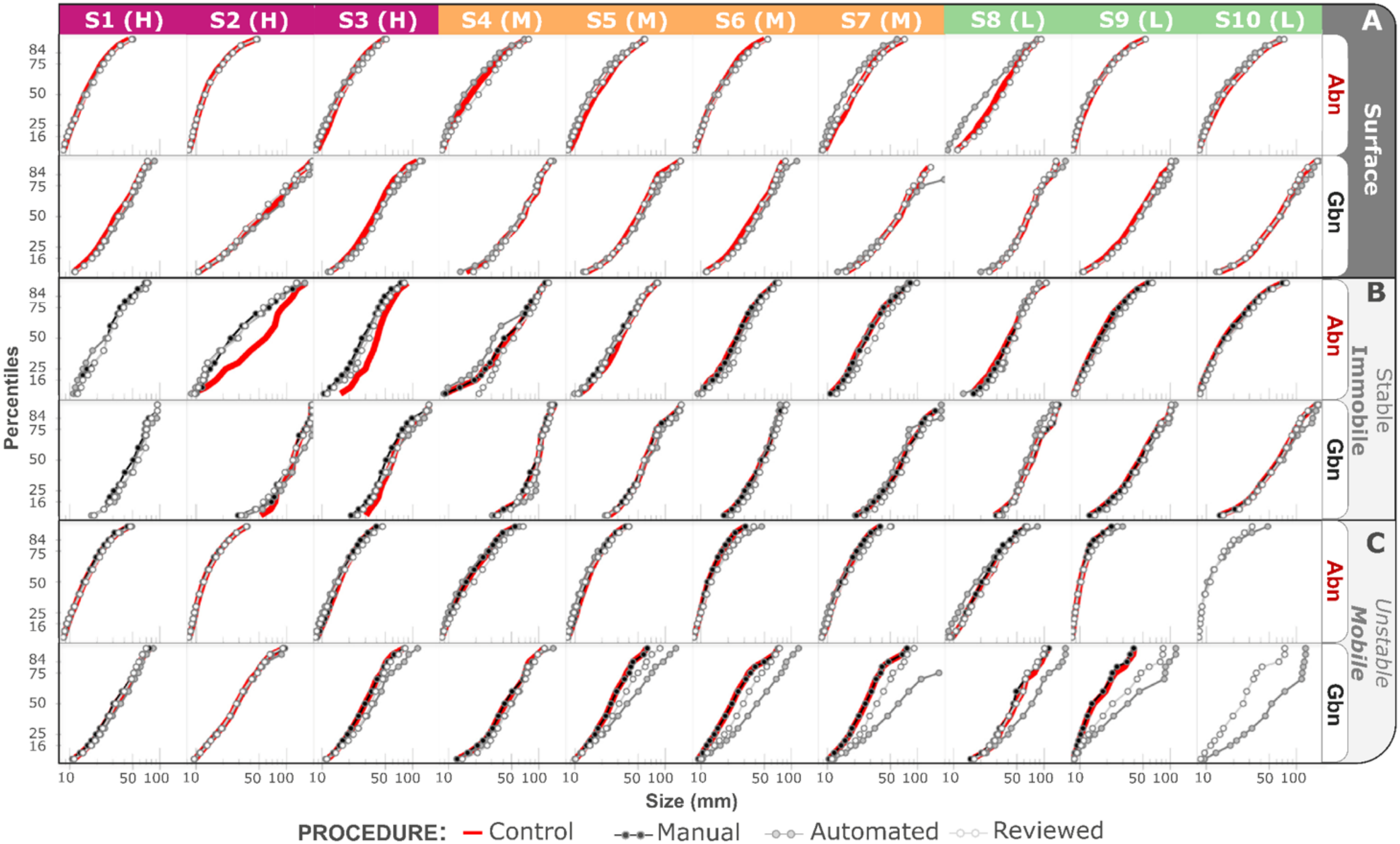

Figure 8: Performance evaluation of the extracted 15 percentile estimates in Abn and Gbn. The 15 points representing the percentile estimates are connected by lines, but the information presented here is not the cumulative distribution frequency. Therefore, the last point at the end of the lines in Abn and Gbn does not correspond to the same size on the x-axis. The last point corresponds to the D95 and not the Dmax (100 %). (A) Surface visible grain percentiles estimates for automated (grey dots) and reviewed (white dots) delineation procedures compared to control data (red solid line). Data in Abn (top) and Gbn (bottom). (B) *Immobile* and *mobile* (C) grain percentiles estimates for *manual* (black dots), *automated* (grey dots), and *reviewed* (white dots) delineation procedures compared to control data (red solid line). Data in Abn (top) and Gbn (bottom)

4.2.2.1 Manual procedure performance It should be remembered that in the *manual* procedure (manual delineation + automatic classification) it is exactly the same grains that are being compared with the control set since this one was obtained via manual delineation + visual classification. Consequently, errors are solely due to the classification model. The *immobile* and *mobile* frequency estimation residuals in Abn and Gbn are between 2.5 and -2.5% (Figure 7 B and C - Manual). The samples with the highest error are the 'highest mobility' samples (S1 to S4). These samples are composed of between 87% and 100% newly deposited *mobile* particles. Sometimes a new particle is deposited in a location where previously a particle had a similar shape and size although it is not the same. Unfortunately, the difference in area and shape is too small to be considered as different (i.e., *mobile*), and they are therefore misclassified as *immobile*. The residuals of the other group samples (medium and low) are lower because there is less turnover of particles and therefore the error due to similar shape is less likely to occur. On the other hand, *immobile* particles are only rarely misclassified as *mobile* in the manual delineation.

4.2.2.1.1 Immobile Distribution Percentiles from the *manual* delineation procedure are underestimated for high intensity events. In Figure 8 B - Abn, for samples S1 to S3, the black points are shifted to the left compared to the continuous solid red line (control data). This is because there are very few *immobile* particles in these control samples (between 0 and 13%, Table 1 and Figure 3 C Abn blue area) and they are often of relatively large size; however, the procedure will identify small *immobile* particles in fractions between 8 mm and 32 mm due to similar shape, so the *immobile* GSD will be refined by adding fines at the beginning of the distribution. The *manual* procedure average MAE of *immobile* percentile estimates (visible in Figure 5 E5 Immobile - black bar) for the high intensity samples is 30% while for medium and low intensity samples it is 1.4-3%.

In Gbn, the maximal 2.5% of over-estimation and under-estimation is more likely to be in the intermediate fraction between 22 mm and 64 mm instead of 8 mm to 32 mm as for Abn. The distributions of high intensity events will be less impacted than in Abn from the beginning of the distribution. In Figure 8 B-Gbn, Sample S1 to S3, the black points are much closer to the solid red curve in Gbn than in Abn. The *manual* procedure average MAE *immobile* percentile estimate for high intensity samples in Gbn is 11.5% (two and a half times less than in Abn) while for medium and low intensity samples it is from 0.4-1.3%.

4.2.2.1.2 Mobile distribution On the other hand, the estimation of the *manual* procedure *mobile* percentiles associated to high intensity events will not be affected by large errors because the 2.5% under-estimation for *mobile* grains between 8 and 32 mm or between 22 to 64 mm has little influence on a grain set composed almost exclusively of *mobile* grains (See Figure 3 C-Abn red area, S1 to S4). There is no strong disparity between the samples subject to different intensity. In Figure 8 C - Abn and Gbn, the black points are relatively close to the red solid line. The *mobile* percentiles are estimated with a manual average MAE of 1.5% in Abn, and of 2.5% in Gbn.

4.2.2.2 Automatic and reviewed procedure performance

4.2.2.2.1 Immobile In Abn, the *automated* delimitation procedure shows disparity between the mobility intensity groups. At lower intensity there is under-estimation of fine *immobile* particles because poor particle delineation will often lead to the classification of *non-real* particles as *mobile*. This problem therefore affects medium to low intensity events in a progressive manner. The *reviewed* delineation shows the same pattern (Figure 7 B - Reviewed - Abn) for the fine fraction, but with lower bias. *Immobile* percentile estimate for medium and low intensity events will tend to be slightly over-estimated as the absence of fine particles results in a GSD containing fewer fine fractions, and will shift the start of the distribution towards coarser sizes. However, the high intensity samples show the same error as the *manual* procedure (see Figure 8 B, Abn, grey and white points). Sometimes small, *immobile* grains are detected due to very similar shapes. The distribution is deviated from the beginning towards finer sizes.

In Gbn, under- or over-estimation of frequencies affects coarser grain size classes than in Abn. The percentile estimate will be biased, but only from high percentiles. This time, the *reviewed* delineation reduces the bias and there is less disparity between the sample groups. The *reviewed* distribution in Gbn has more reliable *immobile* percentiles estimation than the *automated* delineation and also than the *reviewed* delineation in Abn. In Figure 5 E5 - Immobile - Abn, the white column (*reviewed* delineation procedure) shows an average MAE of almost 14% while the *automated* delineation shows a lower average MAE of only 7.5%. In Gbn, the MAE for the *reviewed* delineation decreases to 8.7%, and is similar for the 3 groups of samples. There was insufficient time in the rapid 10 min review correction to deal with small particles, while in Abn it is their presence that controls the GSD. They are present in greater numbers than the coarser particles (see Figure 3 C). The frequency of the fine *immobile* fractions up to 16 mm are under-estimated causing a coarser estimate of the beginning of the distribution, then due to the boundary correction process splitting the coarse union of *non-real* intermediate and coarse grains, the rest of the distribution is less under-estimated, so the whole distribution is shifted towards the coarse sizes. The white points in Figure 8 B, Abn are positioned to the right of the red curve for samples S4, and S6 to S10, while in Gbn these are more superposed to the solid red control curve. The *automated* delineation, due to an under-estimation of the fine fraction, will also present a relatively coarse beginning of the cumulative distribution, but as the other fractions are still under-estimated, there will be less over-estimation of the percentile sizes.

4.2.2.2.2 Mobile In Abn, the estimation of *mobile* grain frequencies with *automated* delineation shows disparity between the sample groups (Figure 7 C - Automated - Abn). The lower the intensity, the higher the over-estimation of the grain frequency as *mobile* for grains < 11 mm. In addition to poor particle delineation creating directly *mobile* classification, if there is a misalignment of the two photos, then the small grains in T1 will not necessarily be superimposed on the same *immobile* small grain present in T0, and will be classified as *mobile*. The small grains are therefore more likely to experience this problem. The larger the grain size, the less important the image shift is, as the *immobile* grains always have some portion of the surface overlapping, allowing the centroid of the reference layer (T1) to be located in the polygon of the compared layer (T0). The *reviewed* delineation does not seem to have completely reduced this phenomenon affecting the finest grains. As already mentioned, the review focuses on the coarse grains first. The first percentiles would tend to be under-estimated due to the addition of small *non-real mobile* particles at the beginning of the distribution.

In Gbn, the *automated* delineation (Figure 7 C - Automated - Gbn) shows increasingly over-estimated mobility with increasing grain size up to 17%. The *reviewed* procedure (Figure 7 D - Reviewed - Gbn) seems to allow a better estimation of the distribution frequencies. The *mobile* percentile derived from the fully automated procedure will be highly over-estimated. In Figure 8 C - Gbn, grey dots are strongly shifted to the right, to larger sizes, as the intensity of the event decreases (from S1 to S10). The *reviewed* delineation correction, focusing on the coarse particles to be segmented, strongly reduces these over-estimates (white dots). The *reviewed* delineation procedure reduces the average MAE of the *automated* delineation from 93% to 29%.

Finally, Figure 8 B shows that all three procedures detected *immobile* particles for sample S1, whereas in the control set, 100% of the grains are *mobile*. For the three procedures, the *non-real immobile* grains in question represent between 4 and 5% of the total grain number, with size ranging from 11 to 93 mm and with median size of 25 mm. Opposite, Figure 8 C, sample S10, shows that the *automated* and *reviewed* procedures detected *mobile* grains, whereas in the control set 100% of the grains were *immobile*. This time the *non-real mobile* grains represent between 18 and 38% of the total grain number, a wider range of sizes (8 to 74mm (reviewed) and to 128mm (automated) with a finer median size of 10 mm. The misclassification seems to have involved a lot of small grains, probably due to image misalignment but also a wide range of grain sizes. In Gbn just some few coarse *non-real* and associated misclassified grains will have a lot of influence creating a very coarse *mobile* distribution when no grain is really moving.

To recap, the error in estimating the frequencies of each grain size fraction varies from 0.2-0.3% for *manual* delineation, from 1-1.5% for *reviewed* delineation and from 2-5% for *automated* delineation. The error on the estimation of percentiles is greater due to the accumulation of frequency errors and varies depending on the form of the distribution and the intensity of the event. In Abn the error on percentile estimate will be higher for the low percentiles and decrease for high percentiles. Meanwhile, Gbn will have more error on the high percentiles. The average MAE (corresponding to the D_{50} percentile MAE) varies from 0.9-2.7% for the *manual* procedure (all percentiles are evaluated with a MAE below 10%), from 7.3-29% for the *reviewed* procedure and from 7.4% to 93% for the *automated* delimitation. Finally, there are less errors when estimating *immobile* grain-size distributions (i.e., stable parts of the bed) than *mobile* ones.

4.3 Fractional dynamics

The fractional stability corresponds, for a given fraction, to the proportion of grains or surface area that remains *immobile* and, complementarily, the fractional mobility corresponds to the *mobile* proportion. The grains of the given fraction have similar surface areas, so the *mobile* and *immobile* proportions are almost identical to those calculated in terms of the number of grains (Abn). As the fractional study only focuses on each individual grain fraction, the estimates of the *immobile* proportion and *mobile* proportion are inversely proportional. In Figure 5 E3, for each procedure, the average error is almost identical between the Abn or Gbn forms and between fractional *mobility* or *immobility*. The predictions of the three procedures are shown only in Abn in Figure 9 A. The red solid line represents the control data. It corresponds to the boundary of the red and blue columns from Figure 3 D, while the black, grey and white points correspond to the predictions obtained via the *manual*, *automatic* and *reviewed* procedures respectively.

4.3.1 Manual procedure performances (classification model only)

The average MAEof the *manual* procedure for low and medium intensity samples is 1.3% (Figure 5 E3 Immobile – Abn). The black dots in Figure 9 A for samples S4 to S10 are almost perfectly superimposed on the continuous control curve. In contrast, the high intensity samples show an under-estimation of the *mobile* proportion and conversely an over-estimation of the *immobile* proportion. The black points are shifted to the right of the red reference curve. The average MAE for this group is of 8.7%. The reason for this is the same as mentioned before i.e., newly deposited particles may be of similar shape to those present before the event, leading to a classification as *immobile* instead of *mobile*. The average MAE of the *manual* procedure is 2.3%.

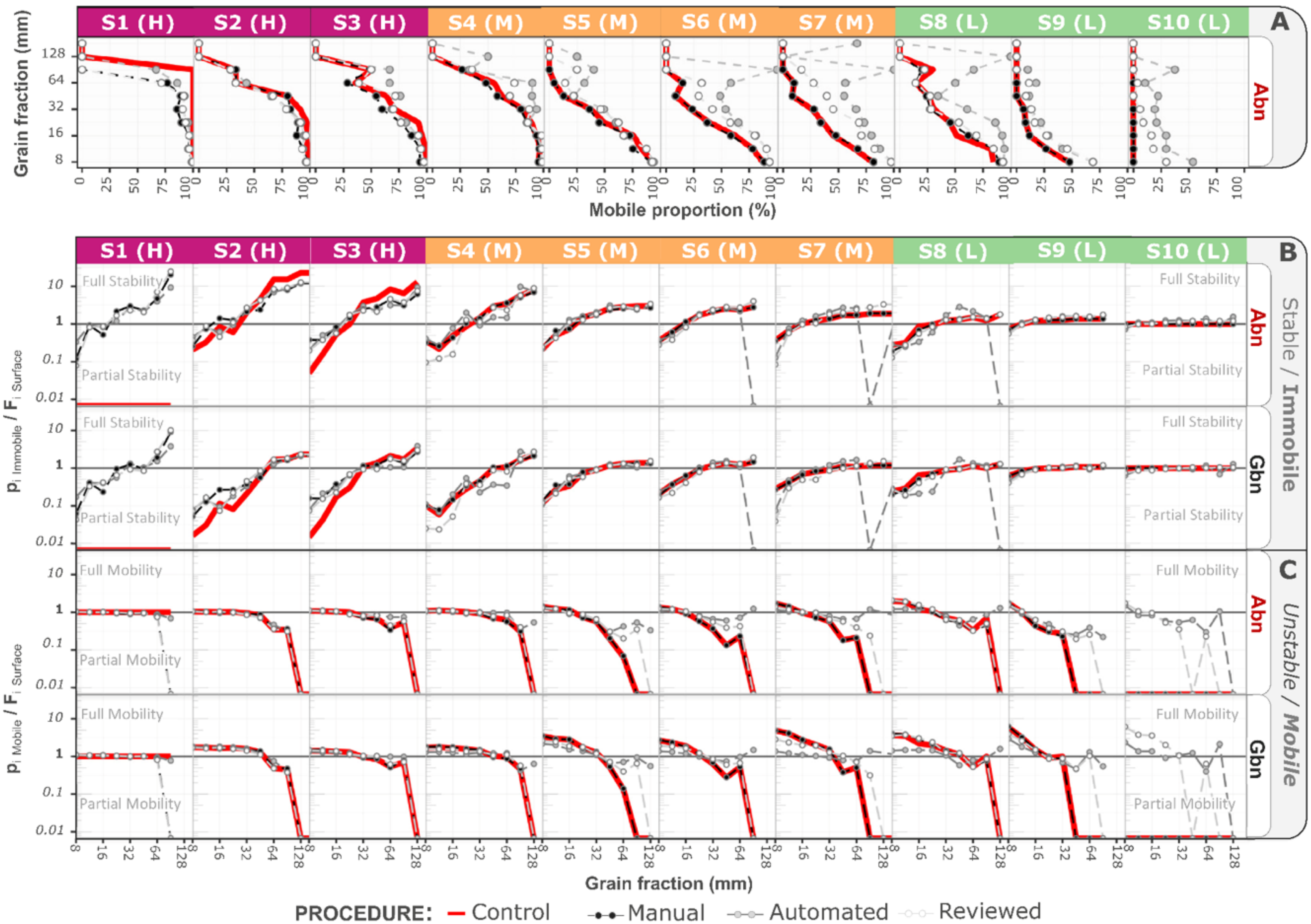

Figure 9: (A) Fractional *mobility/immobility* proportion estimate in Abn for *manual* (black dots), *automated* (grey dots) and *reviewed* (white dots), delineation procedure compared to control data (red solid line). The red solid line corresponds to the boundary of the red and blue columns from Figure 3 D. Data are only in Abn due to similarity with Gbn. (B) Relative fractional *stability* (immobility) ratio estimates and (C) relative fractional mobility (instability) ratio estimates. Where, $p_{i\ Immobile}$ is the proportion of each size fraction i present in the whole *immobile* surface grain category and $p_{i\ Mobile}$ in the whole *mobile* surface grain category, F_i is the proportion of each size fraction i in the whole surface bed sediment. Data in Abn (top) and Gbn (bottom).

4.3.2 Automated and reviewed performance

With *automated* delineation (Figure 9 A - grey dots), the *mobile* proportions of low and medium intensity samples are over-estimated. The grey points are shifted to the right with respect to the red solid reference curve. This phenomenon is more important for grain fractions above 45 mm. The very large errors in the coarse fractions do not accurately reflect the true amount of error. Very few particles are present in the coarse fractions (see Table 1 or Figure 3 D), so the presence or absence of a single grain yields very large errors. *Mobile* over-estimation of coarse grains is explained by the coarse *non-real* particles' identification. If these delineation errors are not the same between the two images, very coarse polygons may be superimposed on smaller real particles in the other image. This has the effect of artificially increasing the number of *mobile* coarse and intermediate grains. For high mobility intensity samples, it is the opposite, the *mobile* particles proportions are under-estimated. As mentioned above, these samples contain very few *immobile* particles i.e., the appearance of a particle misclassified as *immobile* rapidly increases the percentage of errors. Furthermore, the large number of new particles increases the probability in which new and old particles have similar shapes although they are not actually the same particles. The *automated* procedure average MAE over all samples is 20.3%.

The *reviewed* procedure shows the same patterns (e.g., over-estimation of *mobile* proportion for low and medium intensity events and under-estimation of high intensity events) but with lower residuals (smaller distance between red curve and white dots). The coarser fractions no longer show errors, thanks to the boundary correction mainly made on the most visible large grains. The *reviewed* procedure average MAE is 8%.

Once again, grains are considered *mobile* in sample S10, whereas the control set does not show any. The error decreases with increasing grain size. With the revised delineation, up to 25% of the small grains are considered *mobile*. This finding is discussed later in the text.

4.4 Relative fractional dynamics

The relative stability (or mobility) ratio corresponds, for a given fraction, to the proportion that this fraction represents in all the *immobile* (or *mobile*) grains, divided by the proportion that this fraction represents in all the grains forming the surface (*immobile* + *mobile*). If the ratio is equal to or greater than 1, the grain fraction is considered fully stable (or fully *mobile*) while when the ratio is less than 1 the fraction is considered partially stable (or partially *mobile*). The predictions, in both Abn and Gbn form, of the three procedures are shown in Figure 9 B for relative bed stability (*immobility*) and Figure 9 C for relative bed *mobility*. Again, the red solid line represents the control data (manual delineation + visual classification), while the black, grey and white points correspond to the predictions obtained via the *manual*, *automated* and *reviewed* procedures respectively.

4.4.1 Relative stability ratio

The three procedures, *manual*, *automated* and *reviewed*, show the same patterns in Abn and Gbn (Figure 9 B) and performances (Figure 5 – E4 – Immobile). The high intensity samples are the least well estimated. The fine fractions are estimated to be more stable than in the control set (dots higher than control curve), while the coarse fractions are estimated to be less stable than in the control set (dots lower than control line). In Gbn, deviation from the control set shows the same pattern as in AbN but with a higher deviation from the control curve (dots are more distant from the control line than in Abn).

It should be noted that despite the difference in ratios compared to the control set, the classification as partially *immobile* (<1) and fully *immobile* (≥1) is still good. The *manual* procedure provided a correct stability categorization (full/partial) in Abn in 91% of the relative grain fraction stability estimates, and 94% in Gbn. The *automated* procedure provided a correct stability categorization (full/partial) in Abn of 84% and 77% in Gbn. The *reviewed* procedure provided a good stability categorization (full/partial) in Abn of 88% and 87% in Gbn.

4.4.2 Relative mobility ratio

Unlike the immobility ratio, the mobility ratio performance estimates are variable across the three procedures but each procedure produces similar performance in either Abn or Gbn (Figure 5 – E4 – Mobile, Abn and Gbn area almost identical). The *manual* procedure worked well: the black dots in Figure 9 C are almost perfectly aligned with the control curve, and the *manual* procedure provided a correct *mobility* categorization (full/partial) in 91% of the relative grain fraction mobility estimates in Abn and 93% in Gbn. The *automated* and *reviewed* procedures showed good estimates in both Abn and Gbn for high intensity events (grey and white dots close to control line for S1 to S4). In contrast, for the medium intensity events, the small fractions are considered relatively less *mobile* (grey points below the control curve) while the larger fractions are considered relatively more *mobile* (grey points above the control curve). The *reviewed* procedure (white points) shows less difference with the control curve. Overall, the *automated* procedure provided a correct *mobility* categorization (full/partial) in 82% of the relative grain mobility estimates in Abn and 75% in Gbn, while the *reviewed* procedure provided a correct *mobility* categorization (full/partial) in 88% in Abn and 87% in Gbn.

5 Discussion

5.1 Performance limitation and recommendation

5.1.1 Manual procedure

The *manual* delineation + automatic classification, assessing only classification error, yielded good performances compared to the control dataset for all approaches E1 to E5. The MAE averages (for approaches E1, E2, E3 and E5) are between 0.2 and 2.5%. Other metrics are given in supplementary material Table **S**1 to Table **??**. Whether the data are expressed as Abn or Gbn, the performances are similar.

The surface area and eccentricity shape likeness thresholds have been set in PhotoMOB based on a trained data set, but can be user-defined. If the *PhotoMOB* procedure is to be used on another river, it may be possible to carry out two or three pairs of control photos (with *manual* delineation + visual classification) in order to establish whether the automatic classification model we provide is capable of providing similarly acceptable results with respect to a new control set.

It should be noted that the analysis developed in this paper does not provide information on the possible differences between what the operator can measure by the photographic method and the actual or real stability/mobility. An experiment in a controlled environment would be required to obtain a real dataset. Here, the control dataset was elaborated with what was visible from the photo, i.e., it is a visual photo interpretation, the best that can be expected from the photographic method.

5.1.2 Automatic procedure

The fully *automated* procedure (*automated* delineation followed by automatic classification) represents the total error of the procedure in achieving correct grain segmentation and classification. The MAE averages for the approaches E1, E2, E3 and E5 are between 2 and 93%. There is a disparity in performance between the different samples (error of precision) and errors are always greater in the Gbn form, with high impact from large polygons unifying several grains. It should be noted that the photo pairs used in this study (see Figure 3 A -post) were not optimal and came from a set of old photos not acquired for this particular analysis. For instance, *PhotoMOB* has not been developed to perform on partially painted or partially wetted photos creating areas of differing brightness and colours within a photo. A partially painted photo has the same order of magnitude of error as a photo not protected from direct sunlight (see companion paper for further details on this).

As already discussed in the companion paper, two solutions can drastically improve *automated* grain delineation, and therefore the subsequent revision effort: (1) Before photographing the square at post-event time, it can be advisable to paint the area again so that both photos are painted. The aim is to reduce the complexity of the photo, i.e., to reduce the details of the image to only grain boundaries. (2) In the near future we plan to implement the new open-source software library ImageGrains (Mair et al., 2023) in the *PhotoMOB* workflow. An example of the performance of the application of this new library on our photos is available in the supplementary materiel of the companion paper. For the moment, this new algorithm has not been trained on partially painted photos, but we have a dataset to do so. This would further facilitate the protocol we are proposing. However, despite adequate paint and/or implementation of this new grain segmentation algorithm, some error will inevitably remain.

5.1.3 Reviewed procedure

The *reviewed* procedure (*automated* delimitation corrected in 10 minutes followed by boundary revision + automatic classification), shows average MAEs for E1, E2, E3 and E5 between 1 and 29%. Other performance metrics are given in supplementary material from Table **S**1 to Table **??**. A 10-minute correction per photo greatly reduce the errors. The performance gains (compared to the fully *automated* procedure i.e., white vs grey columns Figure 5) are stronger in the Gbn form. Errors are reduced by 60% in Gbn and by 30% in Abn. There is a disparity in performance between different intensity groups. Due to small sample sizes, there were exceptionally large percentage errors on fractions with small numbers of particles, such as the percentage of *immobile* particles in high intensity samples. This had a strong impact on the average error shown in Figure 5. In reality, these classification errors concern only a few grains. In order to solve this problem, after the automatic classification of the grains, the user can symbolize with a certain colour the few grains classified as *immobile* as in Figure 10. In this way, the user can quickly walk around the image and locate these particles and change the attribute field from *immobile* to *mobile*. The inverse *mobile*/*immobile* way can be applied to low mobility intensity samples.

Figure 10 shows samples S1 and S10 with the two pre- and post- photos in transparency on top of each other, where 6 types of errors are pointed out. Recommended strategies during the boundary revision to reduce the 6 errors are available in Text S.5.1.3.

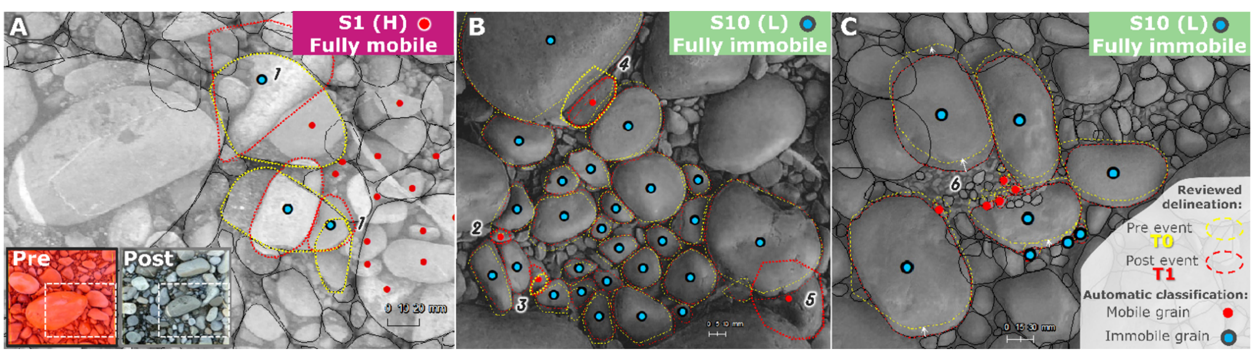

Figure 10: Example of misclassification of grains (A) Error due to the classification model giving *immobile* particles (*1:* similarity threshold too large and maybe not enough shape descriptor used). (B) Misclassification due to *automated* boundary and revision delineation giving *mobile* particle (*2*: small grain found only in a single layer, *3*: relatively small grain identified with slightly different shapes between the two photos, *4*: grain modified by user only in one of the two layers, *5*: user forgets to redraw a grain in one of the two layers. (C) Misclassification due to photo misalignment (*6*: the centroid of the small grain in T1 is not superimposed on the grain in T0 although they are indeed the same). This photo alignment is not the one reported in this study, it is just an example to show the effect of a bad alignment.

However, respecting the best practices during photo collection phase i.e., (i) painting the square before each shot, (ii) protecting the area to be photographed from direct sunlight, (iii) taking the photos as perpendicular to the ground as possible, contributes to an easier, faster and good photo alignment and allows *PhotoMOB* to generate quite good automatic delimitation, thus reducing the effort of boundary correction afterwards. Moreover, correcting the pre and post polygon layers simultaneously, rather than 10 minutes one after the other, could further reduce errors thanks to consistent shape correction between the two layers.

Organizing data, applying filters in GIMP, scaling, aligning the photos, applying the *PhotoMOB toolbox part 1*, correcting the grain boundaries, applying the *PhotoMOB toolbox part 2*, equates to 1-hour desk work per set of paired photos. The objective of the *PhotoMOB* procedure is to automate all of the individual subsequent steps that an operator would have to perform to produce grain delineation and classification in a GIS. Part 1 of *PhotoMOB* described in the companion paper corresponds to the automation of more than 260 successive actions, while Part 2 presented in this paper corresponds to the automation of more than 100 successive actions. The processing of two photos automated by the *PhotoMOB* toolbox to quantify the dynamics represents more than 620 successive actions. These actions should be repeated for each pair of photos per event. The realisation of this procedure in GIS allows the user to control all processes and to check the quality of the results and make corrections. Finally, we believe that implementing the ImageGrains (Mair et al., 2023) algorithm would reduce the processing time for both pre- and post-event images to well under an hour and perhaps even eliminate the need to paint the patches (see example in companion paper, Part 1).

5.2 Immobility, Stability, Mobility, and Instability

The stability of the bed corresponds to the undisturbed, unchanged area. That is, the area that does not exhibit deposition or erosion as a result of a hydrological event. Once the *immobile* grains have been identified, the proportion of the stable zone and the distribution frequency of its *immobile* grain fractions can be determined. The concept of stability/instability is more attributed to the description of the sampled surface, while the concepts of immobility/mobility are attributable to the grain. Care must be taken because with the method we are describing, subtle difference between stability and immobility may exist. It can happen that a particle is considered *immobile* while the area is unstable.

Let's take the example of Figure 11 A. The hydrological event caused entrainment of four small particles present in T0, which have therefore become part of the bedload, and the appearance of a new relatively large particle in T1 (classified as *mobile*). In terms of stability (grey area) and instability (red area), the classification of the pre- and post-event layers are valid, both layers show instability at this location. But looking at the competence of the flow and understanding what (size) grains are *mobile* and *immobile*, then there is a problem. The large particle was slightly visible at T0, so it could be considered as part of the surface sediment. It was not part of the bedload and deposited, but appeared due to bed scour.

Assuming that the *automated* delineation will be corrected by the operator, two situations are possible. In the first one, the coarse grain could only be delineated in the post-event layer (T1). The result will be a classification as *mobile*, which is "false". In the second case, the operator might want to make this large particle also appear in the pre-event layer since it is guessable in T0 and perfectly visible in T1. In this case, this grain will end up classified as *immobile*, which is "true". In both cases, it is problematic to rely on the post-event layer (T1).

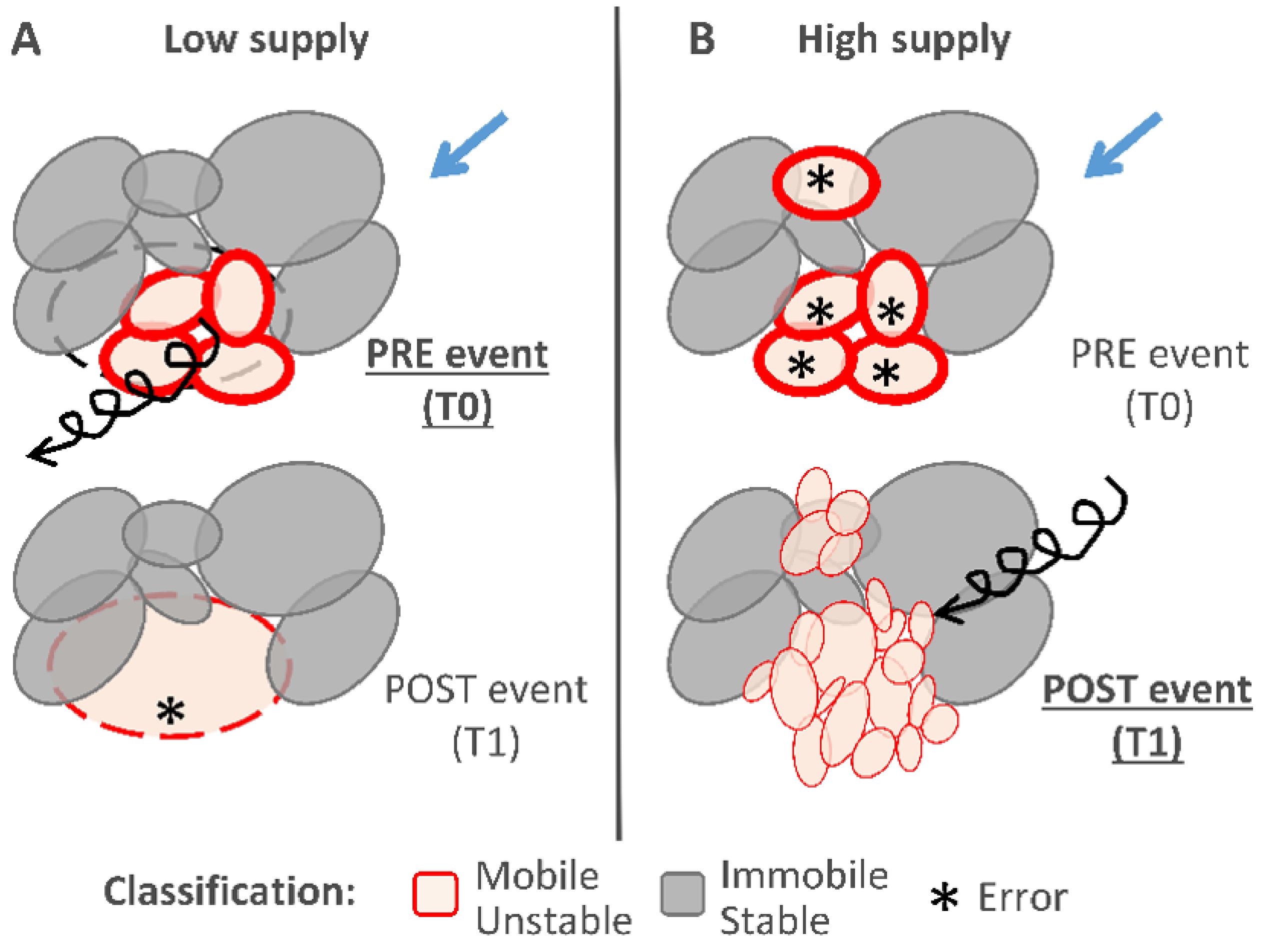

Figure 11: Sketch illustrating probable misjudgements of grain dynamics. (A) In the context of low sediment supply, grains newly appearing in T1 due to surface erosion are classified as *mobile*. The use of the T0 layer classification is recommended for analysing the sediment dynamics. (B) In a context of significant sediment supply, grains previously apparent in T0 can be classified as *mobile*, although it is not certain that they have been transported, perhaps simply covered. The use of the T1 classification is recommended to analyse the sedimentary dynamics.

In the first case, the large grain is classified as *mobile*, which is not true. It will strongly influence the GSD of the *mobile* grains (which can be used as a proxy for the GSD of the bedload). This will lead to a strong over-estimation of the size of the high *mobile* percentiles, even more so if the results are expressed as Gbn. This is one of the factors that explains the highest error in the *reviewed* procedure for the Gbn form (white dots in Figure 7 C and white columns in Figure 5 E5). In the second case, it will be classified as *immobile* (grey instead of red), which is the "reality". But this will lead to the area being considered as stable (undisturbed), which is not true since some grains were eroded.

In the context of low sediment supply, whether from the point of view of stability/instability or immobility/mobility, it would be preferable not to draw the large particle at T0 and to rely on the classification obtained with this pre-event layer (T0) since it does not seem to present any problem. The four small grains are well *mobile* and contribute to bedload, while represent an unstable surface.

In the context of a greater sediment transport rate, schematically represented in Figure 11 B, other subtleties appear. The five small particles present in T0 are no longer visible in T1. Whether one relies on the classification of the pre- or post-event layer, the area is considered unstable, which is "true". On the other hand, it is not certain whether the five small particles in T0 were *mobile* as part of the bedload, or that they remained *immobile* and were covered by new ones. In T1, however, the new visible grains are likely to have been part of the bedload, and to have been deposited here. In the context of significant sediment supply, it will be necessary to rely on the classification obtained from the post-event layer (T1) to quantify both stability/instability and immobility/mobility correctly.

5.3 Use of data

In order to study the sediment dynamics as quickly and reliably as possible, the procedure to be followed and the recommendations listed here and in the rest of this paper are summarized in Figure 12. The processing of the images with the GIS *toolbox PhotoMOB part 1 and 2* generates a shapefile with information for each grain, in pre- and post-event, of its shape characteristics (area, perimeter, *a*-axis, *b*-axis, orientation, rectangularity, eccentricity, roundness, compactness) as well as its classification (*immobile*/*mobile*). The attribute table of these layers is also saved in text format. A web or desktop application based on R language and shiny package (R Core Team, 2022; Chang et al., 2023) , called *PhotoMOB Extractor*, has been developed to analyse the data from the text files and to allow the user to quickly and easily obtain the outputs mentioned in Figure 1 (C1, C2, C4, E1, E2, E3, E4, E5) in both Abn and Gbn form. Depending on the objectives of the study for which the photographic method can be used and the data with which it can be coupled, either the Abn or Gbn form may be preferable.

From a stability/instability point of view, perhaps more related to ecological studies, it will probably be preferable to think in terms of stable or unstable surfaces and therefore use the Gbn form. From a sediment transport dynamics point of view, both forms seem to be useful, the choice will depend on the objectives sought. However, it seems that the Abn form is adequate if the photographic observations are to be linked to mobility or travel distance observation of tracer grains from a pre-defined (painted) patch area. This is because the tracer particles available to be entrained and thus subsequently traced are pre-selected as all surface particles within a pre-defined area. On the other hand, if the dynamics observed via photographs are to be related to other data such as pebble counts, bulk samples, bedload samples obtained by in situ sampling, then the Gbn form would be the most appropriate. Moreover, percentile values may be used in sediment transport equation that have been generally established using Gbn data measured by square holes. In case the compared Gbn data are coming from square holes binned *b*-axis measurement (template, sieve), the apparent *continuous b′*-axis value obtained by the photographic method should be converted based on the flatness of the grains of the studied river (see details in companion paper Part 1).

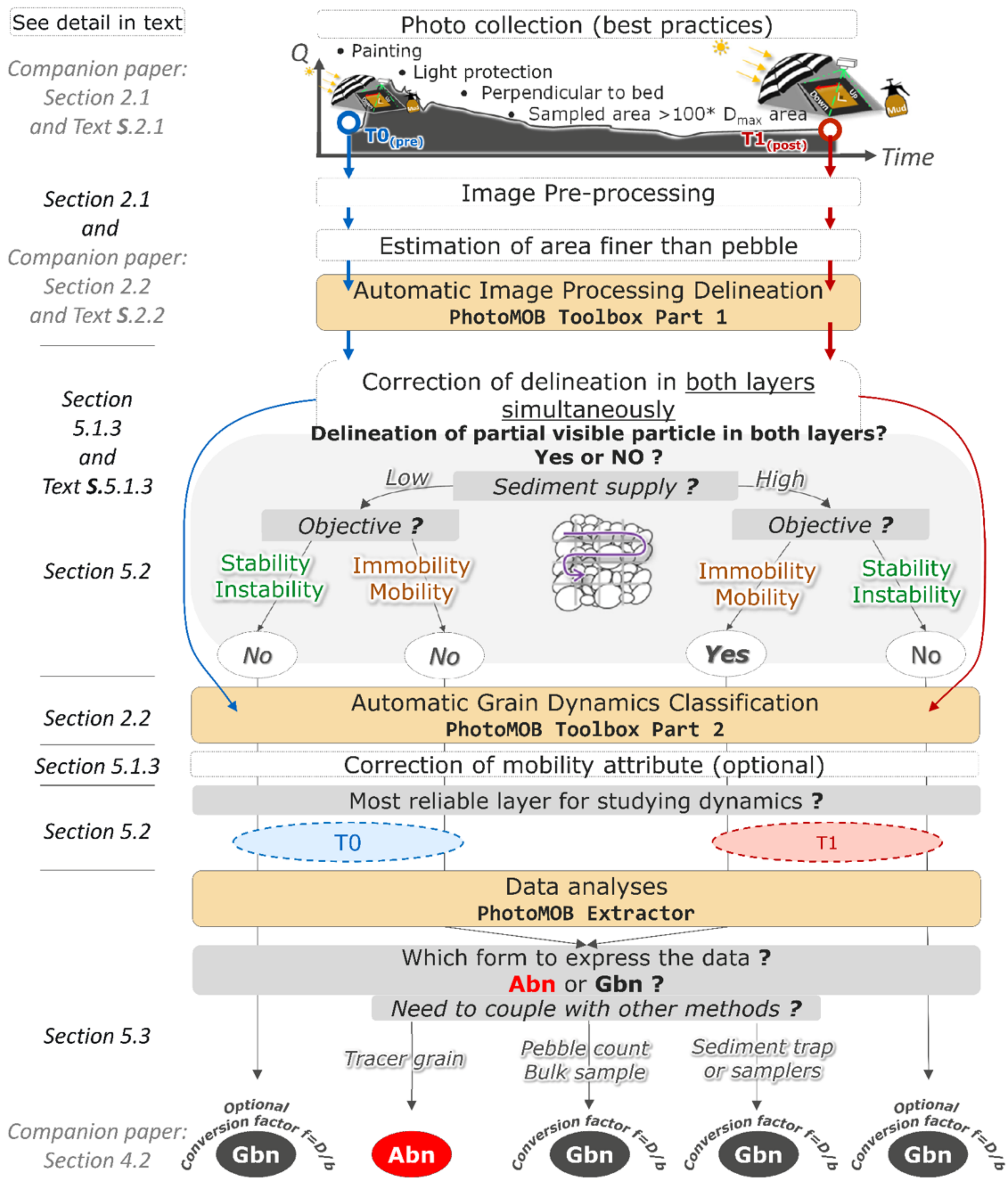

Figure 12: Illustration of the successive stages and recommendations required to extract grain size and dynamics data from photographic method. The yellow boxes represent the automated steps developed in the pair of paper.

6 Concluding remarks

The performance analysis of *PhotoMOB* to characterise particle dynamics in gravel bed rivers shows an acceptable agreement with the control data set. The classification error (mean absolute error) due only to the classification model on perfectly delineated particles (*manual* procedure) is less than 3% for all the outputs examined. The *reviewed* procedure (automated delineation manually revised in 10 min + automated classification) gives a general bed and fractional grain dynamics (stability/mobility) estimates with a mean absolute error of around 8% in both Area-by-number and Grid-by-number GSD form. The relative fractional dynamic as partial or full is well estimated at 87-88% (Abn-Gbn). *Mobile* and *immobile* percentiles are estimated with MAE ranging between 13.7 - 7.3% in Abn and between 8.5 and 28.7% in Gbn.

The photographic method we present has several advantages:

(1) It provides information on bed *mobility* as well as bed *stability*. The latter is generally not covered by other methods.

(2) The data extracted from the photos can be compared with other existing studies thanks to the availability of the data in Gbn form. However, it is important to ensure a large enough sampled area and use *b*-axis size adequate conversion, based on the average grain flatness, in order to compare data from photos and data from measurements using square holes' template or sieves.

(3) If the sampled surfaces are large enough to represent the entire grain-size distribution, even the coarsest fractions, then it will be possible to correctly assess the fractional dynamics of coarse fraction and the maximum *mobile* diameters. Moreover, repeated photographic observations of the same area for hydrological events of different intensity can allow the development of mobility models for each grain size fraction. For a given fraction, the incipient motion threshold can be determined when a hydrological event generates a given minimum *mobile* proportion of the grains in that fraction. Whereas the full mobility threshold can be determined when an event causes 100 % of the *mobile* grain of that fraction or its relative mobility ratio is ≥ 1.

(4) After 1-hour processing (single operator), a lot of information is available (output Figure 1 C and E1). This is faster than the pebble count method (Wolman, 1954), which requires two operators to work at least one hour two different days to just get surface GSD. The estimation of the *mobile* proportion of each grain fraction is faster and more reliable than the time effort to search for *mobile* grains downstream of a painted patch by two operators having to locate and measure all visible grains, where often the return rate is very low.

(5) *PhotoMOB* can be coupled with other types of observations and measurements (painted tracer, pebble count, sediment traps, pit tags) to compensate some of their limitations.

(6) Obtaining the correct categorization of grains can be improved by implementing new algorithms for better grain segmentation.

(7) The protocol is flexible as the grain boundary can be easily corrected and the grain classification too. The user is therefore free to analyse the texture and dynamics of all the grains or to select and create subsets of the grains in the study area and extract their characteristics by group.

Following the steps developed in this pair of papers and the recommendations summarised in Figure 1 and Figure 12, *PhotoMOB* provides an aid to the observation and analysis of sediment dynamics, in a consistent manner, across time and space at the scale of the grain and morphological unit.

Code availability

The processing of the images with the ArcGIS desktop toolbox PhotoMOB part 1 and 2 generates shapefile with for each grain, in pre- and post-event, its shape characteristics (area, perimeter, *a*-axis, *b*-axis, orientation, rectangularity, eccentricity, roundness, compactness) as well as its classification (immobile/mobile). The attribute table of these layers is also saved in text format. A web and desktop application based on R language and shiny package (R Core Team, 2022; Chang et al., 2023), called PhotoMOB Extractor, has been developed to analyse the data from the text files and to allow the user to quickly and easily obtain the outputs mentioned in Figure 1 (C1, C2, C4, E1, E2, E3, E4, E5) in both AbN and GbN form. The actual and future version of the PhotoMOB toolbox as well as the PhotoMOB Extractor App are available with documentation at https://shiny.fannyville.com/PhotoMOB_Tool.html. The toolbox is currently only available for ArcGIS desktop, but will be soon converted to ArcGIS Pro and, additionally, our intention is to convert to the open source QGIS.

Acknowledgments

This research was undertaken under the MorphHab (PID2019104979RB-I00/AEI/10.13039/501100011033) and MorphPeak (CGL201678874-R/AEI/10.13039/501100011033) research projects funded by the Spanish State Research Agency (Ministry of Science and Innovation) and the European Regional Development Fund Scheme (FEDER). The first author has a grant funded by the Ministry of Economy, Industry and Competitiveness, Spain (BES-2017-081850). Damià Vericat is a Serra Húnter Fellow at the University of Lleida. The Fluvial Dynamics Research Group –RIUS is a consoli-dated group recognized by the Generalitat de Catalunya (2021 SGR 01114). We thank Al-exandre Moron for building the square frame and María Eugenia Benito for providing feed-back concerning the development of the PhotoMOB toolbox and Extractor application user interface.

CRediT authorship contribution statement

Fanny Ville: Conceptualization, Methodology, Investigation, Data curation, Formal analysis, Visualization, writing original draft, Writing – review & editing.

Colin Rennie: Methodology, Supervision, Writing – review & editing.

Ramon J. Batalla: Funding acquisition, Methodology, Supervision, Writing – review & edit-ing.

Damià Vericat: Funding acquisition, Methodology, Supervision Writing – review & editing.

Data availability statement

Control, manual, automated and reviewed dataset made of identified and classified grains used in PhotoMOB error assessment, as well as example files to use in the PhotoMOB Ex-tractor app are available under: https://zenodo.org/records/10038313

Declaration of competing interest

The authors declare that they have no conflict of interest.

References

Andrews, E. and G. Parker (1987). "Formation of a coarse surface layer as the response to gravel mobility". In: *Sedient transport in gravel-bed rivers*. Ed. by C. R. Thorne, J. C. Bathurst and R. D. Hey. John Wiley & Sons , pp. 269-325. https://cir.nii.ac.jp/crid/1574231874050281856.

Ashworth, P. J., R. I. Ferguson, P. E. Ashmore, et al. (1992). "Measurements in a Braided River chute and lobe: 2. Sorting of bed load during entrainment, transport, and deposition". In: *Water Resources Research* 28.7. ISBN: 0878148965, pp. 1887-1896. DOI: 0043-1397/93/92WR02748.

Brenna, A., N. Surian, and L. Mao (2019). "Virtual Velocity Approach for Estimating Bed Material Transport in Gravel-Bed Rivers: Key Factors and Significance". In: *Water Resources Research* 55.2. Citation Key: Brenna2019a, pp. 1651-1674. DOI: 10.1029/2018WR023556.

Cerney, D. L. (2010). "The Use of Repeat Photography in Contemporary Geomorphic Studies: An Evolving Approach to Understanding Landscape Change: Repeat photography use in geomorphic studies". In: *Geography Compass* 4.9, pp. 1339-1357. DOI: 10.1111/j.1749-8198.2010.00376.x. https://onlinelibrary.wiley.com/doi/10.1111/j.1749-8198.2010.00376.x.

Chang, W., J. Cheng, J. Allaire, et al. (2023). *shiny: Web application framework for R*. Citation Key: shiny. https://CRAN.R-project.org/package=shiny.

Church, M. and M. A. Hassan (2002). "Mobility of bed material in Harris Creek: MOBILITY OF BED MATERIAL IN HARRIS CREEK". In: *Water Resources Research* 38.11. DOI: 10.1029/2001WR000753. http://doi.wiley.com/10.1029/2001WR000753.

Cobb, D. G., T. D. Galloway, and J. F. Flannagan (1992). "Effects of Discharge and Substrate Stability on Density and Species Composition of Stream Insects". In: *Canadian Journal of Fisheries and Aquatic Sciences* 49.9, pp. 1788-1795. DOI: 10.1139/f92-198. http://www.nrcresearchpress.com/doi/10.1139/f92-198.

Dey, S. and S. Z. Ali (2019). "Bed sediment entrainment by streamflow: State of the science". In: *Sedimentology* 66.5. Citation Key: Dey2019, pp. 1449-1485. DOI: 10.1111/sed.12566.

Downes, B. J., A. Glaister, and P. S. Lake (1997). "Spatial Variation in the Force Required to Initiate Rock Movement in 4 Upland Streams: Implications for Estimating Disturbance Frequencies". In: *Journal of the North American Benthological Society* 16.1, pp. 203-220. DOI: 10.2307/1468252. https://www.journals.uchicago.edu/doi/10.2307/1468252.

Duncan, M. J. and A. M. Suren (1999). "Assessment of Streambed Stability in Steep, Bouldery Streams: Development of a New Analytical Technique". In: *Journal of the North American Benthological Society* 18.4, pp. 445-456. DOI: 10.2307/1468377. https://www.journals.uchicago.edu/doi/10.2307/1468377.

Gibbins, C. (2015). "Coupling Biological and Physical Processes: The Ecological Significance of River Channel Hydraulics and Fluvial Dynamics". In: *Rivers – Physical, Fluvial and Environmental Processes*. Ed. by P. Rowiński and A. Radecki-Pawlik. Series Title: GeoPlanet: Earth and Planetary Sciences DOI: 10.1007/978-3-319-17719-9_19. Cham: Springer International Publishing, pp. 479-496. https://link.springer.com/10.1007/978-3-319-17719-9_19.

Gibbins, C., E. Scott, C. Soulsby, et al. (2005). "The relationship between sediment mobilisation and the entry of Baetis mayflies into the water column in a laboratory flume". In: *Hydrobiologia* 533.1-3, pp. 115-122. DOI: 10.1007/s10750-004-2401-1. http://link.springer.com/10.1007/s10750-004-2401-1.

Gibbins, C., D. Vericat, and R. J. Batalla (2007). "When is stream invertebrate drift catastrophic? The role of hydraulics and sediment transport in initiating drift during flood events". In: *Freshwater Biology* 52.12, pp. 2369-2384. DOI: 10.1111/j.1365-2427.2007.01858.x. https://onlinelibrary.wiley.com/doi/10.1111/j.1365-2427.2007.01858.x.

Gilbert, G. K. and E. C. Murphy (1914). *The Transportation of Debris by Running Water*. DOI: 10.3133/pp86 Citation key: gilbert1914. California Water Science Center, U.S. Geological Survey, p. 263. DOI: 10.3133/pp86. https://pubs.usgs.gov/publication/pp86.

Hassan, M. A. and P. Ergenzinger (2003). "Use of Tracers in Fluvial Geomorphology". In: *Tools Fluv. Geomorphol.* John Wiley & Sons, Ltd. Chap. 14, pp. 397-423. ISBN: 9780470868331. DOI: https://doi.org/10.1002/0470868333.ch14. https://onlinelibrary.wiley.com/doi/abs/10.1002/0470868333.ch14.

Hassan, M. A. and A. G. Roy (2016). "Coarse particle tracing in fluvial geomorphology". In: *booktitle*. Ed. by G. M. Kondolf and H. Piégay. 1st ed. DOI: 10.1002/9781118648551.ch14. Wiley, pp. 306-323. DOI: 10.1002/9781118648551.ch14. https://onlinelibrary.wiley.com/doi/10.1002/9781118648551.ch14.

Komar, P. D. (1987). "Selective gravel entrainment and the empirical evaluation of flow competence". In: *Sedimentology* 34.6, pp. 1165-1176. DOI: 10.1111/j.1365-3091.1987.tb00599.x. https://onlinelibrary.wiley.com/doi/10.1111/j.1365-3091.1987.tb00599.x.

López, R., F. Ville, C. Garcia, et al. (2023). "Bed-material entrainment in a mountain river affected by hydropeaking". In: *Science of The Total Environment* 856, p. 159065. DOI: 10.1016/j.scitotenv.2022.159065. https://linkinghub.elsevier.com/retrieve/pii/S0048969722061642.

Lorang, M. S. and F. R. Hauer (2003). "Flow competence and streambed stability: an evaluation of technique and application". In: *Journal of the North American Benthological Society* 22.4, pp. 475-491. DOI: 10.2307/1468347. https://www.journals.uchicago.edu/doi/10.2307/1468347.

MacKenzie, L. G., B. C. Eaton, and M. Church (2018). "Breaking from the average: Why large grains matter in gravel-bed streams: Breaking from the average". In: *Earth Surface Processes and Landforms* 43.15, pp. 3190-3196. DOI: 10.1002/esp.4465. https://onlinelibrary.wiley.com/doi/10.1002/esp.4465.

Mair, D., G. Witz, A. Do Prado, et al. (2023). "Automated finding, segmenting, and measuring of grains in images of fluvial sediments –the potential of transfer learning in deep neural networks". In: *Submitted to Earth Surf. Process. Landforms*. DOI: 10.31223/X51H31. DOI: 10.31223/X51H31. https://eartharxiv.org/repository/view/5523/.

Mao, L. and M. A. Lenzi (2007). "Sediment mobility and bedload transport conditions in an alpine stream". In: *Hydrological Processes* 21.14, pp. 1882-1891. DOI: 10.1002/hyp.6372. https://onlinelibrary.wiley.com/doi/10.1002/hyp.6372.

Mao, L., L. Picco, M. A. Lenzi, et al. (2017). "Bed material transport estimate in large gravel-bed rivers using the virtual velocity approach". In: *Earth Surface Processes and Landforms* 42.4. Citation Key: Mao2017a, pp. 595-611. DOI: 10.1002/esp.4000.

Matthaei, C. D. and C. R. Townsend (2000). "Long-term effects of local disturbance history on mobile stream invertebrates". In: *Oecologia* 125.1, pp. 119-126. DOI: 10.1007/PL00008883. http://link.springer.com/10.1007/PL00008883.

Miller, M. C., I. N. McCAVE, and P. D. Komar (1977). "Threshold of sediment motion under unidirectional currents". In: *Sedimentology* 24.4, pp. 507-527. DOI: 10.1111/j.1365-3091.1977.tb00136.x. https://onlinelibrary.wiley.com/doi/10.1111/j.1365-3091.1977.tb00136.x.

Parker, G. (2008). "Transport of Gravel and Sediment Mixtures". In: *Sedimentation Engineering*. DOI: 10.1061/9780784408148.ch03 Citation Key: Parker2008. Reston, VA: American Society of Civil Engineers, pp. 165-251. DOI: 10.1061/9780784408148.ch03. http://ascelibrary.org/doi/10.1061/9780784408148.ch03.

Peckarsky, B. L., A. R. McIntosh, S. C. Horn, et al. (2014). "Characterizing disturbance regimes of mountain streams". In: *Freshwater Science* 33.3, pp. 716-730. DOI: 10.1086/677215. https://www.journals.uchicago.edu/doi/10.1086/677215.

Quinlan, E., C. Gibbins, I. Malcolm, et al. (2015). "A review of the physical habitat requirements and research priorities needed to underpin conservation of the endangered freshwater pearl mussel Margaritifera margaritifera". In: *Aquatic Conservation: Marine and Freshwater Ecosystems* 25.1. Citation key: quinlan2015, p. 107–124. ISSN: 10527613. DOI: 10.1002/aqc.2484. http://doi.wiley.com/10.1002/aqc.2484.

Team, R. C. (2022). *R: A language and environment for statistical computing*. Citation Key: R_stat. Vienna, Austria: R Foundation for Statistical Computing. https://www.R-project.org/.

Team, T. G. D. (2019). *GIMP*. Citation Key: Team. https://www.gimp.org.

Vázquez-Tarrío, D., E. Fernández-Iglesias, M. Fernández García, et al. (2019a). "Quantifying the Variability in Flow Competence and Streambed Mobility with Water Discharge in a Gravel-Bed Channel: River Esva, NW Spain". In: *Water* 11.12. Citation Key: vasques2019quantifying, p. 2662. ISSN: 2073-4441. DOI: 10.3390/w11122662. https://www.mdpi.com/2073-4441/11/12/2662.

Vázquez-Tarrío, D., E. Fernández-Iglesias, M. Fernández García, et al. (2019b). "Quantifying the Variability in Flow Competence and Streambed Mobility with Water Discharge in a Gravel-Bed Channel: River Esva, NW Spain". In: *Water* 11.12. Citation Key: vasques2019quantifying, p. 2662. ISSN: 2073-4441. DOI: 10.3390/w11122662. https://www.mdpi.com/2073-4441/11/12/2662.

Vericat, D., R. J. Batalla, and C. Garcia (2008). "Bed-material mobility in a large river below dams". In: *Geodinamica Acta* 21.1-2. Citation Key:vericat2008b, pp. 3-10. DOI: 10.3166/ga.21.3-10. https://www.tandfonline.com/doi/full/10.3166/ga.21.3-10.

Vericat, D., F. Ville, A. Palau-Ibars, et al. (2020). "Effects of Hydropeaking on Bed Mobility: Evidence from a Pyrenean River". In: *Water* 12.1. Citation Key: Vericat2020, p. 178. DOI: 10.3390/w12010178. https://www.mdpi.com/2073-4441/12/1/178.

Wathen, S. J., R. I. Ferguson, T. B. Hoey, et al. (1995). "Unequal Mobility of Gravel and Sand in Weakly Bimodal River Sediments". In: *Water Resources Research* 31.8. Citation Key: wathen1995, pp. 2087-2096. DOI: 10.1029/95WR01229. http://doi.wiley.com/10.1029/95WR01229.

Wilcock, P. R. (1997). "The components of fractional transport rate". In: *Water Resources Research* 33.1, pp. 247-258. DOI: 10.1029/96WR02666. http://doi.wiley.com/10.1029/96WR02666.

Wilcock, P. R. and B. W. McArdell (1993). "Surface-based fractional transport rates: Mobilization thresholds and partial transport of a sand-gravel sediment". In: *Water Resources Research* 29.4, pp. 1297-1312. DOI: 10.1029/92WR02748. http://doi.wiley.com/10.1029/92WR02748.

Wolman, M. G. (1954). "A method of sampling coarse river-bed material". In: *Transactions, American Geophysical Union* 35.6. Citation Key: Woman1954 ISBN: 9780415475976, p. 951. DOI: 10.1029/TR035i006p00951. https://doi.org/10.1029/TR035i006p00951.

S SUPPORTING INFORMATION

Note

Supporting Information for:

PhotoMOB: Automated GIS method for estimation of fractional grain dynamics in gravel bed rivers.

Part 2 : Bed stability and fractional mobility

Contents of this file:

This document provides supplementary material. It is structured using the same headings as the main article to help readers find what they are interested in reading more about. Title followed by the word "none" indicate that no supplementary information is provided for that section.

S.1 Introduction

Bed mobility can be assessed by direct methods such as the *Helley Smith sampler,* Helley and Smith (1971) and *sediment traps*, Bunte and Abt (2001) , and indirect approaches as for instance *tracers* (Church and Hassan, 2002; Hassan and Ergenzinger, 2003; Vázquez-Tarrío and Batalla, 2019) and those based on *visual estimation* (moss, algae's development, (Pfankuch, 1975)) and on *organism density changes* (Schwendel, 2012). All these methods or approaches have limitations in terms of applicability, ease of implementation or accuracy. One inexpensive method, is the use of a painted bed area (i.e. painted tracers, see summary in Hassan and Roy (2016)). A representative area of the bed is painted and then usually photographed to identify each grain and derive the pre-event surface GSD using automated tools such as *Sedimetrics Digital Gravelometer©* (Graham (2005a, 2005b)) or *Basegrain* (Detert and Weitbrecht, 2013). Following a hydrological event, the entrained painted grains can be located downstream and transport distances measured. This method avoids altering natural grain imbrication without limitation of tracer size. However, the majority of measurements generally focus on the downstream particles, while a large amount of information from the original spot location has not been exploited, such as the proportion of the bed surface that is *stable* (*immobile*) for each grain size fraction. It should be noted that in only few studies (e.g., Vericat et al., 2008; Mao and Surian, 2010; Mao et al., 2017), the overall proportion of the bed surface that remained *stable* has been estimated, either visually by changes in painted surface between two photos or by analysing the proportion of pixels that still have paint in a post-event photo. This technique yields the proportion of the sampled bed area that has remained *stable* (not scoured and/or filled), but it can be unreliable if the paint washes off, and it has not as of yet taken into account grain size. Although information on the fractional mobility of each grain size fraction is present in the photo, to our knowledge this has not previously been extracted systematically.

Within this context and limitations, we have developed a semi-automated method for quantifying the stability and mobility of bed grains, based on photographic methods and GIS processing. The paper quantifies its performance.

S.2 The complete PhotoMOB workflow

The objective of the procedure is to compare two photos, of the exact same river bed area, acquired before and after a hydrological event (or a succession of events when it is impossible to access the area).

S.2.1 Grains' detection

None

S.2.2 Characterization of grain dynamics

The categorisation (see Figure **S**1 – B below), by comparing grain located at the same coordinates between the pre- and post-event photo, will be done on sediments from the same section of the river, the two grain shapes are likely to be similar. In order to overcome this problem, five particle shape descriptors were tested (Chaki and Dey, 2019). It is necessary to establish which shape descriptors are most relevant and then to evaluate the relative difference thresholds of these criteria in order to decide whether particles are identical or not. We constructed a training dataset consisting of 10 pairs of pre- (T0) and post- event (T1) photos coming in equal proportions from two rivers of the South Central Pyrenees (Cinca and Ésera). The sedimentary characteristics of these rivers are detailed in the companion paper (Part 1). Each photo was scaled and a projective transformation applied, then the T1 photo was aligned with the T0 photo using control points (identical points between the two photos).

All the particles were manually delimited in the form of polygon shapefiles. More than 12100 particles were delineated. For each particle, we extract five shape descriptors (see Figure **S**1 – B and C above).

(i) The surface area, (ii) the compactness which represents the relationship between the area and the perimeter of the particle:

$$Compactness = 4\pi \times \frac{Area}{Perimeter^2} \tag{S1}$$

Next, (iii) the roundness is obtained using the minimal circle envelope box, in which the roundness is the proportion the particle fills its minimal circle:

$$Roundness = \frac{Area_{Particle}}{Area_{Circle}} \tag{S2}$$

The next two descriptors are obtained using the minimal rectangle bounding box. By creating this box, the length of the axes of the particle is known, which allows the calculation of the (iv) eccentricity which corresponds to the aspect ratio:

$$Eccentricity = \frac{A_{axis}}{B_{Axis}} \tag{S3}$$

Then, (v) the rectangularity which indicates in which proportion the particle is rectangular, i.e. in which proportion the particle fills its minimal rectangle:

$$Rectangularity = \frac{Area_{Particle}}{Area_{Rectangle}} \tag{S4}$$

The polygons delimiting the particles at T1 have been transformed into a point layer, materializing their centroid. This point layer still contains the shape characteristics information at post event time. This T1 point layer has been superimposed on the polygon layer materializing the particles at T0. The T0 shape information (area, compactness, roundness, eccentricity, rectangularity) has been attached to the T1 point overlay. At this stage, the T1 centroid point layer has the paired shape information from T1 and T0 (Figure **S**1). Then the grain degree of likeness is evaluated. For each shape descriptor, the percentage difference is calculated by taking pre-event time as a reference:

$$Shape\ likeness = \frac{Descriptor_{post} - Descriptor_{pre}}{Descriptor_{pre}} \times 100$$

If a T1 particle is not coupled to any T0 particle, then it is considered to be *mobile* (newly arrived). A single operator visually assigned the dynamics status (*immobile* or *mobile*) to each T1 particle listed in the T1 point layer. In total 5479 pairwise particle comparisons were performed. As the particle detection limits may vary slightly between photos or if an operator is using a lower resolution camera, we decided to truncate the particles to 8 mm, decreasing the number of retained comparisons to 4202.

We then used R Core Team (2022) software and the *rpart* package developed by Therneau and Atkinson (2019) to build a classification decision tree model. Among the 4202 pairs, 852 represented *immobile* particles while 3350 represented *mobile* particles. In order not to influence the classification results we randomly eliminated particles classified as *mobile* from our training set to obtain equal proportions of both classes. Of the remaining 1704 particles we used 70% to train different classification trees and kept 30% to test models and select the best one. The simplest tree with good accuracy was preferred. The selected classification model is shown Figure **S**1 – C2 above. The testing accuracy was 87%. The two relevant descriptors are (i) particle area and (ii) eccentricity. The surface area seems to be the first intuitive descriptor. Finally, eccentricity makes sense because even if the images are rotated, translated, with a slightly different scale, the eccentricity ratio should remain similar. If two paired particles have a difference in area greater than 38%, then they are considered to be different (*mobile*). If not, if the difference in eccentricity is greater than 31%, then they are considered to be *mobile*, otherwise they are identical (*immobile*).

Once the particles have been classified, it is possible to derive different types of information. This data can be expressed as the number of grains in the sampled area, i.e. Area-by-number (Abn), or in terms of grain area in the sampled area. The latter is equivalent to the Grid-by-number (Gbn) data form commonly obtained by the pebble-count method (Wolman, 1954). Figure **S**1 - D shows a conceptual example of the possible data that can be obtained from the analysis of photo pairs.

• Taking the surface sediment as a whole (out of 100 %) and the mobility classification or status of each particle (i.e. *mobile* or *immobile*), it is possible to calculate the *immobile* proportion (i.e., bed stability) and the *mobile* proportion (i.e., bed instability) in term of grain number or area (see Figure **S**1 – D5)

• Additionally, because each particle is classified as *mobile* or *immobile*, it is also possible to know frequency distribution of each grain fraction per dynamics status composing the new bed surface (see Figure **S**1 – D6).

• The relative fractional stability (or relative fractional mobility) can also be examined with the ratio p_i/F_i (see Figure **S**1 – D8). In this expression, p_i is the frequency of the *immobile* particle in a given i^{th} size fraction. F_i is the frequency for the given fraction i taking all surface grains as a whole (*immobile* + *mobile*). A value less than 1 indicates partial mobility or stability, depending if p_i is based on the *mobile* or *immobile* grains, whereas a ratio $p_i/F_i \geq 1$ indicates full mobility or stability of the fraction i.

• Finally, taking as two distinct sets the *mobile* and *immobile* particles, it is possible to calculate for each status the frequencies of each fraction, to derive the cumulative frequency and to estimate the percentiles (see Figure **S**1 – D9).

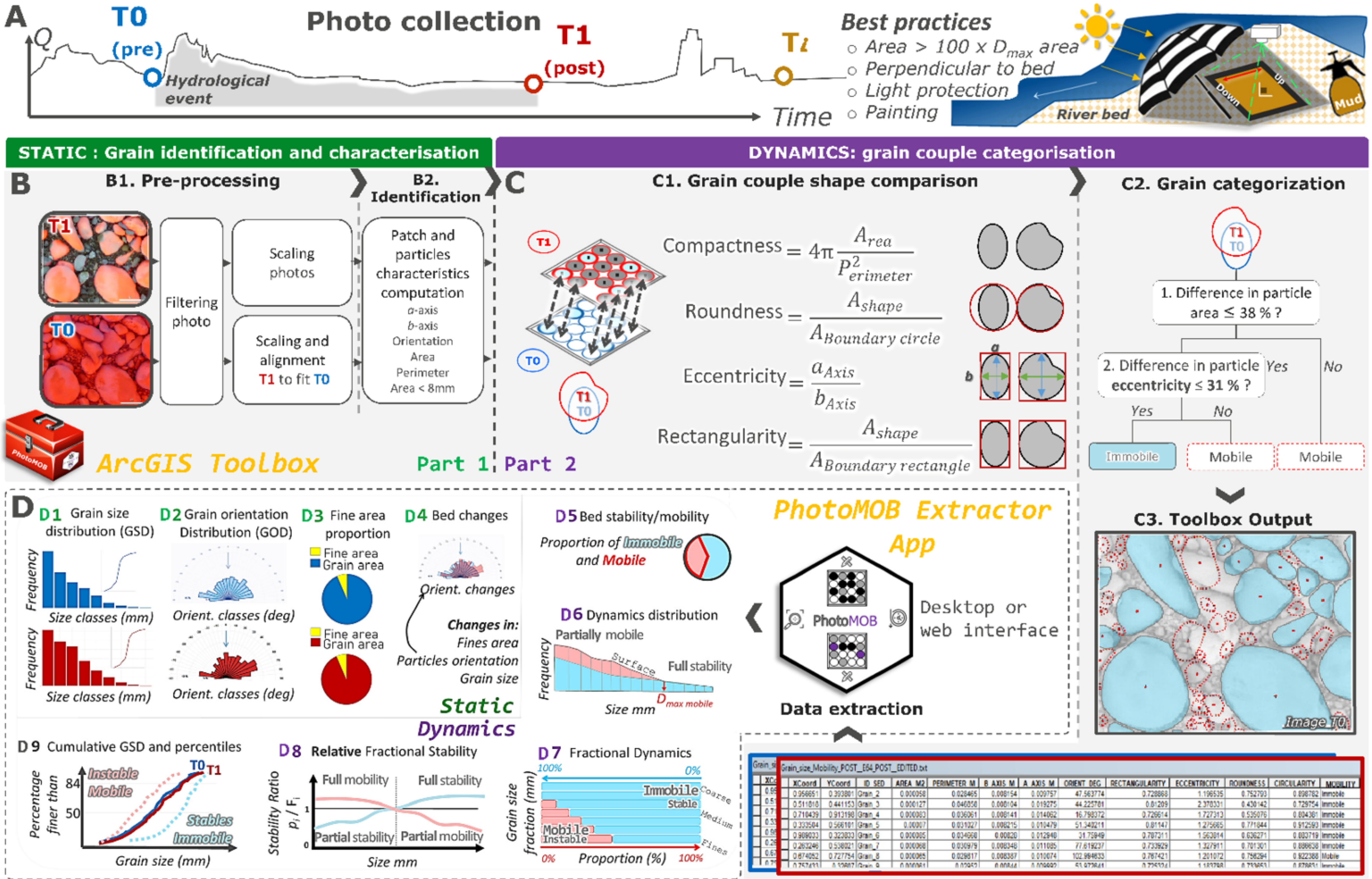

Figure **S**1: Illustration of the workflow required to samples and characterize bed surface (see companion paper, Part 1) and sediment dynamics (developed in this paper). (A) Photo acquisition. *PhotoMOB* toolbox Part 1 for (B) detection of grain and shape characterisation and Part 2 for (C) grain couples' comparison and categorization. (D) Extraction of different possible types of data (static views in green D1 to D4, and dynamic views in purple D5 to D8) facilitated by the *PhotoMOB* Extractor application.

S.2.2.1 Hypothesis and rationale

None

S.2.2.2 Workflow

None

S.3 Performance assessment

None

S.3.1 Control dataset

None

S.3.2 Performance assessment approaches

Figure **S**2 shows an overview of the *reviewed* particle delineation at T0 and T1 (columns A and B), as well as the result of applying the classification model to the *reviewed* delineation at T1, with the photo at T0 in the background (column C). The correction of delineations can still cause classification errors. In the case of *automated* delineation errors and a correction made only on one of the two layers, the shapes of the grains still remain different, leading to misclassification as *mobile* (see Figure **S**2) – M_2). This error is also covered in the *main text* and latter in this document Test S.5.1.3.1.

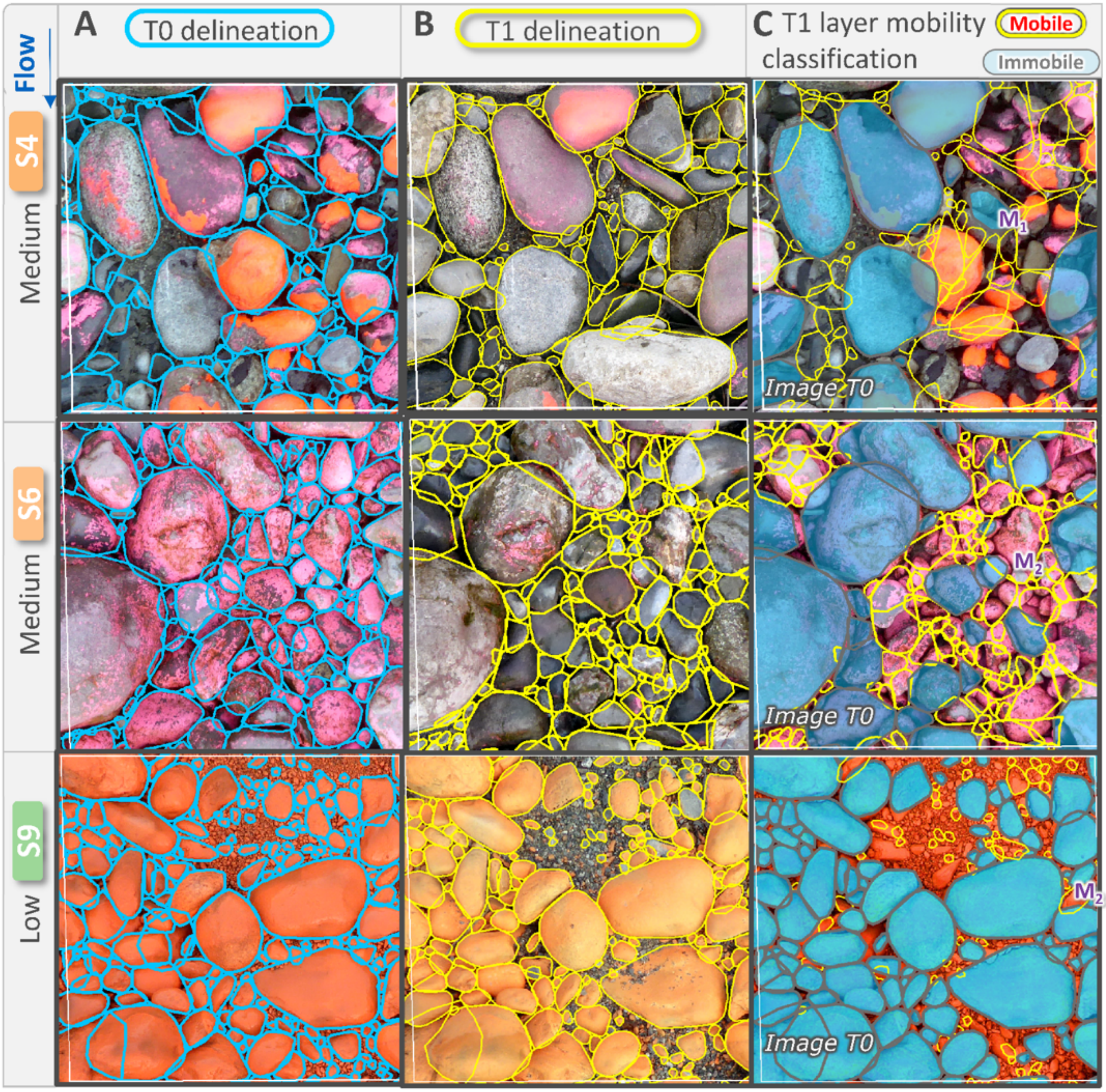

Figure **S**2: Particle *reviewed* delineation results at T0 (A) and T1 (B). (C) Automated particle classification as *immobile* or *mobile* based on T1 classification. The image patches represent approximatively 40cm*40cm and show delineated particles > 8mm. The label 'M' is showing misclassification example. 'M1' correspond a miss classification as *immobile* due to similar shape. 'M2' correspond to a misclassification as *mobile* due to shape correction only in one layer (T0 or T1) leading to different shapes while the particles were *immobile*.

S.4 Results of performance assessment

Average performance procedure metrics (Bias, e, MAE, RMSE) are available below

S.4.1 General bed dynamics

Table **S**1: Bed stability performances (Figure **S**1– D5)

Distribution [a]	Delineation procedure [b]	Procedure Bias (B) [c]		Procedure Irreducible error (e) [c]		Procedure Accuracy error (MAE) [c]		Procedure RMSE [c]	
		Abn %	Gbn %	Abn %	Gbn %	Abn %	Gbn %	Abn %	Gbn %
Bed stability	Manual	2.1	2.7	2.9	3.5	**2.5**	**2.8**	3.6	4.4
	Reviewed	-6.1	-5.1	9.6	8.3	**8.7**	**7.9**	11.4	9.8
	Automated	-14.6	-19.5	15.5	19.0	**16.6**	**21.9**	21.3	27.3

[**a**] The bed stability proportion (number - Abn or area - Gbn) is inversely proportional to bed mobility. The bias for bed mobility will have the opposite sign to those shown here for bed stability. Other metric values will be equal for bed stability or mobility. [**b**] The *manual* procedure corresponds to *manual* delineation + automatic grain categorization, *automated* procedure corresponds to *automated* delineation + automatic grain categorisation, and *reviewed* procedure correspond to *automated* delineation followed by 10 min of boundary correction + automatic grain categorization. [**c**] Average of the bed stability/Instability proportion estimates error over the 10 samples, corresponding to the general procedure errors for each procedure (*manual*, *automated*, *reviewed*). [**d**] Theses value correspond to the column in Figure 5 (*main text*).

S.4.2 Distribution per dynamics status

Table **S**2: Grain size and dynamics status performances (Figure **S**1 – D6)

Distribution[a]	**Delination procedure**[b]	**Procedure Bias (B)**[c,d]		**Procedure Irreducible error (e)**[c]		**Procedure Accuracy error (MAE)**[c,e]		**Procedure RMSE**[c]	
		Abn	**Gbn**	**Abn**	**Gbn**	**Abn**	**Gbn**	**Abn**	**Gbn**
		% *(sd)*	**%** *(sd)*	**%** *(sd)*	**%** *(sd)*	**%** *(sd)*	**%** *(sd)*	**%** *(sd)*	**%** *(sd)*
Surface	Reviewed	0 *1.3*	0.1 *0.9*	1.1 *0.9*	1.4 *0.9*	**1.2** *1*	**1.2** *0.7*	1.5 *1.2*	1.6 *0.9*
	Automated	0 *3*	0.9 *3.8*	1.6 *1.4*	2.3 *1.4*	**2** *2.3*	**3** *3.1*	2.4 *2.7*	3.4 *3.3*
Immobile	Manual	0.2 *0.2*	0.2 *0.2*	0.4 *0.4*	0.3 *0.3*	**0.3** *0.3*	**0.2** *0.2*	0.4 *0.4*	0.4 *0.3*
	Reviewed	-0.6 *0.8*	-0.6 *0.9*	1.3 *1*	1.5 *0.9*	**1.1** *0.9*	**1.4** *0.8*	1.5 *1.3*	1.8 *1*
	Automated	-1.4 *1*	-2.1 *2.7*	1.8 *1.2*	2.8 *1.7*	**1.7** *1.1*	**3.2** *2.1*	2.3 *1.5*	4 *2.5*
Mobile	Manual	-0.2 *0.2*	-0.2 *0.2*	0.4 *0.4*	0.3 *0.3*	**0.3** *0.3*	**0.2** *0.2*	0.4 *0.4*	0.4 *0.3*
	Reviewed	0.6 *1*	0.7 *1*	1.4 *1.4*	1.1 *0.7*	**1.3** *1.2*	**1.1** *1*	1.7 *1.6*	1.4 *1.1*
	Automated	1.5 *2.7*	4.2 *5*	1.8 *1.7*	2.3 *1.5*	**2.1** *2.7*	**4.5** *4.8*	2.5 *3.1*	5.2 *4.8*

a Distribution of surface grains, *immobile* and *mobile*, for the 3 delineation procedures tested. For the surface, the manual and control grains are the same. **b** The manual procedure corresponds to *manual* delineation + automatic grain categorization, *automated* procedure corresponds to *automated* delineation + automatic grain categorisation and *reviewed* procedure correspond to *automated* delineation followed by 10 min of boundary correction + automatic grain categorization. **c** Average of grain frequency errors, for each metric, over the 10 grain fractions, corresponding to the general procedure errors for each procedure (*manual*, *automated*, *reviewed*) and each distribution (surface, *immobile*, *mobile*). The sd represent the standard deviation around the average. A low value indicates a constant error of prediction along grain fraction while greater value indicates disparity of performance estimation along grain fraction. **d** The procedure bias corresponds to the average of the black curve in Figure 7 (main text) while *sd* indicate how constant or not are the black line along grain fractions. **e** The procedure MAE in black bold correspond to the value of the column in Figure 5 (main text)

Table **S**3: Percentiles estimates performances (Figure **S**1 – D9)

Distribution[a]	Delination procedure [b]	Procedure Bias (B) [c]				Procedure Irreducible error (e) [c]				Procedure Accuracy error (MAE) [c, d]				Procedure RMSE [c]			
		mm (sd)		**%** (sd)		**mm** (sd)		**%** (sd)		**mm** (sd)		**%** (sd)		**mm** (sd)		**%** (sd)	
		Abn	**Gbn**	**Abn**	**Gbn**	**Abn**	**Gbn**	**Abn**	**Gbn**	**Abn**	**Gbn**	**Abn**	**Gbn**	**Abn**	**Gbn**	**Abn**	**Gbn**
Surface[e]	Reviewed	0.8 *0.8*	0.6 *1.2*	2 *2.7*	2.3 *2.4*	1.3 *0.7*	2.1 *2.0*	5.2 *1.6*	3.4 *1.5*	1.3 *0.7*	2.1 *1.5*	**5.0** *1.0*	**3.9** *1.6*	1.6 *0.9*	2.5 *1.9*	6.1 *1.3*	4.6 *1.8*
	Automated	-2.8 *1.1*	9.3 *13.0*	-11.0 *4.1*	9.5 *12.7*	3.2 *1.5*	10.3 *14.8*	10.2 *1.6*	12.4 *10.2*	3.2 *1.5*	10.6 *12.1*	**12.3** *2.9*	**13.9** *8.9*	4.3 *1.7*	14.6 *19.1*	15.2 *3.6*	17.7 *13.9*
Immobile	Manual	0.0 *0.3*	-0.1 *0.2*	0.2 *1.1*	-0.3 *0.5*	1.0 *0.4*	0.5 *0.3*	3.3 *1.9*	1.1 *0.9*	0.8 *0.3*	0.4 *0.2*	**2.7** *1.6*	**0.9** *0.7*	1.0 *0.4*	0.6 *0.3*	3.4 *1.9*	1.2 *1.0*
	Reviewed	3.6 *1.4*	3.9 *3.5*	12.5 *3.0*	7.6 *4.4*	3.0 *1.2*	4.7 *5.3*	9.8 *2.2*	6.6 *3.0*	4.0 *1.4*	4.8 *3.2*	**13.7** *3.4*	**8.5** *3.9*	4.7 *1.7*	6.4 *6.0*	16.0 *3.2*	10.3 *4.8*
	Automated	0.0 *1.3*	-0.3 *5.0*	1.5 *3.2*	1.3 *4.5*	2.9 *1.9*	9.2 *8.2*	8.4 *2.9*	11.3 *4.9*	2.5 *1.5*	8.1 *6.8*	**7.4** *2.5*	**10.3** *4.0*	3.1 *2.1*	9.9 *8.9*	9.0 *3.2*	12.1 *5.1*
Mobile	Manual	-0.4 *0.4*	-0.6 *0.6*	-1.4 *1.1*	-1.6 *1.1*	0.6 *0.6*	1.5 *1.5*	1.6 *1.3*	3.1 *2.4*	0.4 *0.4*	1.0 *1.0*	**1.5** *1.1*	**2.5** *1.8*	0.7 *0.7*	1.6 *1.6*	2.1 *1.7*	3.6 *2.5*
	Reviewed	1.4 *1.8*	7.6 *6.0*	5.8 *6.8*	27.0 *13.3*	1.0 *1.0*	6.8 *6.5*	5.1 *2.5*	23.0 *14.1*	1.6 *1.7*	8.8 *7.2*	**7.3** *5.5*	**28.7** *14.0*	1.9 *2.0*	10.4 *8.7*	8.7 *6.0*	36 *18.6*
	Automated	0.8 *3.5*	35.5 *33.9*	1.1 *###*	92.5 *63.4*	1.8 *1.3*	19.4 *21.7*	9.0 *2.2*	53.6 *45.9*	2.2 *2.9*	35.5 *33.9*	**10.1** *6.7*	**92.6** *63.3*	2.7 *3.1*	40.7 *40.0*	12.7 *6.9*	107.5 *77.3*

a Distribution of surface grains, *immobile* and *mobile*, for the 3 delineation procedures tested. For the surface, the manual and control grains are the same. **b** The manual procedure corresponds to *manual* delineation + automatic grain categorization, *automated* procedure corresponds to *automated* delineation + automatic grain categorisation and *reviewed* procedure correspond to *automated* delineation followed by 10 min of boundary correction + automatic grain categorization. **c** Average of percentiles estimate errors, for each metric, over the 15 extracted percentiles, corresponding to the general procedure errors for each procedure (*manual*, *automated*, *reviewed*) and each distribution (surface, *immobile*, *mobile*). The sd represent the standard deviation around the average. A low value indicates a constant error of prediction along percentiles while greater value indicates disparity of performance estimation along percentiles. **d** The procedure MAE in black bold correspond to the value of the column in Figure 5 (main text). The procedure bias corresponds to the average of the black line in Figure 7 (main text) while the sd indicate how constant or not are the black line along grain fractions. **e** The performance of the *automated* and *reviewed* procedures for estimating surface percentiles can be compared with the performance data presented in the companion paper (Part 1).

S.4.3 Fractional dynamics

Table **S**4: Fractional performances (Figure S1 – D7)

Mobility[a]	**Delination procedure**[b]	**Procedure Bias (B)**[c]		**Procedure Irreducible error (e)**[c]		**Procedure Accuracy error (MAE)**[c,d]		**Procedure RMSE**[c]	
		Abn	**Gbn**	**Abn**	**Gbn**	**Abn**	**Gbn**	**Abn**	**Gbn**
		% *(sd)*	**%** *(sd)*	**%** *(sd)*	**%** *(sd)*	**%** *(sd)*	**%** *(sd)*	**%** *(sd)*	**%** *(sd)*
Immobile	Manual	1.6 *1.5*	1.4 *1.3*	3.1 *1.9*	2.7 *1.9*	**2.3** *1.7*	**2.1** *1.7*	3.6 *2.2*	3.1 *2.2*
	Reviewed	-5.7 *3.4*	-6.2 *3.7*	8.3 *4.8*	8.2 *4.8*	**8** *4.6*	**8.3** *4.9*	10.2 *5.6*	10.4 *5.9*
	Automated	-18.4 *11.7*	-20 *11.6*	20.1 *11.3*	20.8 *11.1*	**20.3** *11.1*	**21.6** *11.1*	27.8 *15.1*	29.6 *14.5*
Mobile	Manual	-1.6 *1.5*	-1.4 *1.3*	3.1 *1.9*	2.7 *1.9*	**2.3** *1.7*	**2.1** *1.7*	3.6 *2.2*	3.1 *2.2*
	Reviewed	5.7 *3.4*	6.2 *3.7*	8.3 *4.8*	8.2 *4.8*	**8** *4.6*	**8.3** *4.9*	10.2 *5.6*	10.4 *5.9*
	Automated	17.2 *10.4*	18.8 *10.6*	19.4 *9.9*	20.1 *9.8*	**19.1** *10*	**20.4** *10.2*	26.5 *13.1*	28.3 *12.6*

[a] The *manual* procedure corresponds to *manual* delineation + automatic grain categorization, *automated* procedure corresponds to *automated* delineation + automatic grain categorisation, and *reviewed* procedure correspond to *automated* delineation followed by 10 min of boundary correction + automatic grain categorization. **[b]** Average of the fractional dynamic estimate's errors, for each metric, over the 10 grain fractions, corresponding to the general procedure errors for each procedure (*manual*, *automated*, *reviewed*) and each distribution (*immobile*, *mobile*). The sd represent the standard deviation around the average. A low value indicates a constant error of prediction along grain fractions while greater value indicates disparity of performance estimation grain fraction. **[c]** The procedure MAE in black bold correspond to the value of the column in Figure 5 (main text)

S.4.4 Relative fractional dynamics

Table **S**5: Relative fractional performances (Figure **S**1 – D8)

Mobility[a]	Delination procedure[b]	Procedure Accuracy error[c]	
		Abn	Gbn
		ratio *(sd)*	ratio *(sd)*
Immobile	Manual	**1.10** *0.40*	**1.52** *0.94*
	Reviewed	**1.14** *0.29*	**1.43** *0.82*
	Automated	**1.13** *0.47*	**1.40** *0.97*
Mobile	Manual	**1.00** *0.03*	**1.01** *0.03*
	Reviewed	**1.60** *0.91*	**1.50** *0.91*
	Automatied	**2.84** *2.08*	**2.60** *2.19*

[a] Groups of *immobile* and *mobile* grain, for the 3 delineation procedures tested. **[b]** The *manual* procedure corresponds to *manual* delineation + automatic grain categorization, *automated* procedure corresponds to *automated* delineation + automatic grain categorisation, and *reviewed* procedure correspond to *automated* delineation followed by 10 min of boundary correction + automatic grain categorization. **[c]** Average of the relative fractional dynamic error ratio over the 10 grain fractions, corresponding to the general procedure errors for each procedure (*manual*, *automated*, *reviewed*) and each distribution (*immobile*, *mobile*). The sd represent the standard deviation around the average. A low value indicates a constant error of prediction along grain fractions while greater value indicates disparity of performance estimation grain fraction. Theses value correspond to the column in Figure 5 (main text)

S.5 Discussion

S.5.1 Performance limitation and recommendation

S.5.1.1 Manual procedure

None

S.5.1.2 Automatic procedure

None

S.5.1.3 Reviewed procedure

S.5.1.3.1 Recommendation for the revision of the grain contour Figure 10 A (*main text*) is a localized view of the result of the *reviewed* procedure obtained on sample S1. The black outline represents the T0 or PRE event grain (see small Pre square on the left). The background image represents the T1 or POST event grain (see in T1 the small square on the right). The dots (blue and red) represent some examples of comparison results. Only *mobile* grains are expected (red dot). However, the classification results in *immobile* grains (blue dot). Here, the grains concerned were correctly delineated. The yellow and red layers highlight the pre- and post- event misclassified contours of the grains. The shapes of these grains are too similar to be considered as different. In this case, the correction of the grain boundaries will never correct these errors. The surface and eccentricity likeness thresholds are too large in these cases, perhaps the addition of another shape descriptor could have allowed a correct classification. After the classification, a check and correction of the attribute field can be considered to inverse the classification results.

Figure 10 B (*main text*) shows errors, which this time are theoretically avoidable in the *reviewed* procedure. The picture shows the sample S10 where only *immobile* grains are expected (blue dot), but the classification gave some grains as *mobile* (red dot). The point numbered 2 represents a small particle detected in the post-event (red contour). However, this small particle does not appear in the pre-event layer (no yellow contour). The image processing leading to the amplification of the edges by the application of filters and the image binarization (see companion paper, Part 1) resulted in the detection of a particle identified as smaller than 8 mm, therefore discarded. This small particle, present only in the post-event, is therefore considered *mobile* (i.e., new). The operator could either delete this small red polygon to avoid creating a *mobile* particle or add a small yellow polygon. Point 3 represents a particle detected in both photos but whose shapes are too different to be classified as identical. The operator would have to modify one of them to allow classification as identical. These two types of error, 2 and 3, are related to the *automated* delimitation and to the lack of time of the operator who preferred to correct larger, more visible particles and did not linger on the small grains.

Point 4 corresponds to a particle identified in both layers. However, it seems that in the pre-event layers (yellow outline), the particle has been entirely redrawn by hand by guessing its part hidden under the adjacent much larger particle in the upper left. In the post-event layer (red outline), the particle has not been modified. This has generated polygons of too different shapes to be considered as one and the same particle. This time, the misclassification comes from the operator's correction and not from the original *automated* delimitation. Similarly, point 5 shows a grain that in both the T0 and T1 automatic delineations was joined to the adjacent larger grain. During the review process, grains were separated and the grain at point 5 was only redrawn in the T1 image, which mistakenly resulted in a *mobile* interpretation. As for error in point 4, it is therefore advisable to first generate the *automated* delineation of the grains of the two photos to then display both to correcting them at the same time with consistency to avoids such errors (4 and 5) and allows to run through both layers at the same time rather than one after the other, which is a time grain. In order to be efficient during this correction work, it is advisable to apply a virtual grid to the photos and to carry out the correction line by line (or column by column). We believe that the implementation of the ImageGrains algorithm (Mair et al., 2023) for grain detection could greatly eliminate these problems.

Finally, Figure 10 C (main text) shows a type of error that is not related to the *automated* delimitation or its correction. Once again, the image corresponds to sample S10 where all the grains are *immobile* (blue dot). However, some small grains are given *mobile* (red dot). The grains appear in both pre and post layer and are correctly delimited by the *automated* delimitation. However, the post image is not correctly aligned with the pre image. It is possible to see the shift on the coarse grain with small white arrows. The yellow outlines are shifted upwards with respect to the red outline. The offset is between 5 and 10 mm. The centroids of T1 polygons are therefore no longer superimposed on the small yellow polygons. They are considered *mobile*. This alignment between the pair of photos of S10 is not the one presented in this paper. During the alignment of these photos, we saved the two not fully aligned photos and then generated the automatic delineation and correction in 10 minutes to see the impact of the misalignment. Misalignment can increase the fractional mobility of fine grain fractions by 2/3. For example, the well aligned sample S10 (presented in this paper) showed a proportion of *mobile* grain between 8 and 11 mm of more than 25% (*main text*, Figure 8 A, S10). With less well aligned photos, as seen in Figure 10 C, this fraction of grain can show a *mobile* proportion of more than 75%. As a reminder, 0% was expected. A correct photo alignment is essential to obtain accurate data on fractional stability/mobility, especially for small fractions. Worth to notice that such a small grain may constitute marginal bedload that may have a role in rivers affected by frequent low-intensity flows such as for instance hydropeaks, hence putting the entrainment threshold very low, but in any case with ecosystemic implications (Gibbins et al., 2007). It can sometimes seem difficult to align the photos properly. Often this is because the photos are not taken from the same point of view, especially when images are not perfectly nadir. Two different angles of view make it difficult to get a correct uniform alignment on the entire image. It might be possible to add a small spirit level to the camera. This could be a less cumbersome and quicker alternative for operators than a structure or a tripod to get a correct perpendicular picture from the ground.

S.5.2 Immobility, Stability, Mobility, and Instability

None

S.5.3 Use of data

None

S.6 Concluding remarks

None

Suplementary references

Bunte, K. and S. R. Abt (2001). *Sampling Surface and Subsurface Particle-Size Distributions in Wadable Gravel- and Cobble-Bed Streams for Analyses in Sediment Transport , Hydraulics , and Streambed Monitoring*. Vol. 00. DOI: 10.1017/CBO9781107415324.004 PMID: 21939040. Ft. Collins, CO: U.S. Department of Agriculture, Forest Service, Rocky Mountain Research Station. DOI: 10.1017/CBO9781107415324.004. https://www.fs.usda.gov/treesearch/pubs/4580.

Chaki, J. and N. Dey (2019). *A Beginners Guide to Image Shape Feature Extraction Techniques*. Ed. by L. Taylor & Francis Group. DOI: 10.1201/9780429287794 Citation Key: Dey2020. CRC Press. DOI: 10.1201/9780429287794. https://www.taylorfrancis.com/books/9781000034301.

Church, M. and M. A. Hassan (2002). "Mobility of bed material in Harris Creek: MOBILITY OF BED MATERIAL IN HARRIS CREEK". In: *Water Resources Research* 38.11. DOI: 10.1029/2001WR000753. http://doi.wiley.com/10.1029/2001WR000753.

Detert, M. and V. Weitbrecht (2013). "User guide to gravelometric image analysis by BASEGRAIN". In: *Advances in river sediment research*. Ed. by S. Fukuoka, H. Nakagawa, T. Sumi and H. Zhang. Citation Key: Detert2013a ISBN: 978-1-315-85658-2 Pages: 165 Place: London Publication title: Advances in river sediment research Type: Other conference item tex.size: 8 p.. CRC Press, pp. 1789-1796. https://people.ee.ethz.ch/~basement/baseweb/download/tools/basegrain/ISRS2013_MDEWV_225.pdf.

Gibbins, C., D. Vericat, and R. J. Batalla (2007). "When is stream invertebrate drift catastrophic? The role of hydraulics and sediment transport in initiating drift during flood events". In: *Freshwater Biology* 52.12, pp. 2369-2384. DOI: 10.1111/j.1365-2427.2007.01858.x. https://onlinelibrary.wiley.com/doi/10.1111/j.1365-2427.2007.01858.x.

Graham, D. J., I. Reid, and S. P. Rice "Automated Sizing of Coarse-Grained Sediments: Image-Processing Procedures". In: *Mathematical Geology* 37.1. Citation Key: Graham2005a, pp. 1-28. DOI: 10.1007/s11004-005-8745-x. http://link.springer.com/10.1007/s11004-005-8745-x.

Graham, D. J., S. P. Rice, and I. Reid "A transferable method for the automated grain sizing of river gravels". In: *Water Resources Research* 41.7. Citation Key: Graham2005b, pp. 1-12. DOI: 10.1029/2004WR003868. http://doi.wiley.com/10.1029/2004WR003868.

Hassan, M. A. and P. Ergenzinger (2003). "Use of Tracers in Fluvial Geomorphology". In: *Tools Fluv. Geomorphol.* John Wiley & Sons, Ltd. Chap. 14, pp. 397-423. ISBN: 9780470868331. DOI: https://doi.org/10.1002/0470868333.ch14. https://onlinelibrary.wiley.com/doi/abs/10.1002/0470868333.ch14.

Hassan, M. A. and A. G. Roy (2016). "Coarse particle tracing in fluvial geomorphology". In: *booktitle*. Ed. by G. M. Kondolf and H. Piégay. 1st ed. DOI: 10.1002/9781118648551.ch14. Wiley, pp. 306-323. DOI: 10.1002/9781118648551.ch14. https://onlinelibrary.wiley.com/doi/10.1002/9781118648551.ch14.

Helley, E. J. and W. Smith (1971). "Development and calibration of a pressure-difference bedload sampler". In: *US Dep. Inter. Geol. Surv. Water Resour. Div.*, p. 21. http://pubs.er.usgs.gov/publication/ofr73108.

Mair, D., G. Witz, A. Do Prado, et al. (2023). "Automated finding, segmenting, and measuring of grains in images of fluvial sediments, the potential of transfer learning in deep neural networks". In: *Submitted to Earth Surf. Process. Landforms*. DOI: 10.31223/X51H31. DOI: 10.31223/X51H31. https://eartharxiv.org/repository/view/5523/.

Mao, L., L. Picco, M. A. Lenzi, et al. (2017). "Bed material transport estimate in large gravel-bed rivers using the virtual velocity approach". In: *Earth Surface Processes and Landforms* 42.4. Citation Key: Mao2017a, pp. 595-611. DOI: 10.1002/esp.4000.

Mao, L. and N. Surian (2010). "Observations on sediment mobility in a large gravel-bed river". In: *Geomorphology* 114.3. Publisher: Elsevier B.V. Citation Key: Mao2010, pp. 326-337. DOI: 10.1016/j.geomorph.2009.07.015. http://dx.doi.org/10.1016/j.geomorph.2009.07.015.

Pfankuch, D. (1975). *Stream reach inventory and channel stability evaluation*. Northern Region Forest Service, US Department of Agriculture, Washington, DC. https://wildlandhydrology.com/resources/docs/Assessment/Pfankuch_1975.pdf.

Schwendel, A. C. (2012). "Measurement of stream bed stability characteristics relevant to lotic ecosystems". In: *Management of mountain watersheds*. Ed. by J. Krecek, M. J. Haigh, T. Hofer and E. Kubin. Citation Key: Schwendel2012 DOI: 10.1007/978-94-007-2476-1_9. Dordrecht: Springer Netherlands, p. 113–122. DOI: 10.1007/978-94-007-2476-1_9. https://doi.org/10.1007/978-94-007-2476-1_9.

Team, R. C. (2022). *R: A language and environment for statistical computing*. Citation Key: R_stat. Vienna, Austria: R Foundation for Statistical Computing. https://www.R-project.org/.

Therneau, T. and B. Atkinson (2019). *rpart: Recursive Partitioning and Regression Trees*. Citation Key: therneauRpartRecursivePartitioning2019. https://CRAN.R-project.org/package=rpart.

Vázquez-Tarrío, D. and R. J. Batalla (2019). "Assessing Controls on the Displacement of Tracers in Gravel-Bed Rivers". In: *Water* 11.8. Citation key: vasquez2019, p. 1598. DOI: 10.3390/w11081598. https://www.mdpi.com/2073-4441/11/8/1598.

Vericat, D., R. J. Batalla, and C. Garcia (2008). "Bed-material mobility in a large river below dams". In: *Geodinamica Acta* 21.1-2. Citation Key:vericat2008b, pp. 3-10. DOI: 10.3166/ga.21.3-10. https://www.tandfonline.com/doi/full/10.3166/ga.21.3-10.

Wolman, M. G. (1954). "A method of sampling coarse river-bed material". In: *Transactions, American Geophysical Union* 35.6. Citation Key: Woman1954 ISBN: 9780415475976, p. 951. DOI: 10.1029/TR035i006p00951. https://doi.org/10.1029/TR035i006p00951.